

# ornl

ORNL/TM-13128

Examination of Babcock & Wilcox Tubes  
After Exposure in an Industrial  
Heat Exchangers

**OAK RIDGE  
NATIONAL  
LABORATORY**

LOCKHEED MARTIN



J. R. Keiser  
M. K. Ferber  
H. F. Longmire  
L. R. Walker  
D. L. Hindman

**MASTER**

*Low*

**DISTRIBUTION OF THIS DOCUMENT IS UNLIMITED**

MANAGED AND OPERATED BY  
LOCKHEED MARTIN ENERGY RESEARCH CORPORATION  
FOR THE UNITED STATES  
DEPARTMENT OF ENERGY

ORNL-27 (3-96)

#### **DISCLAIMER**

This report was prepared as an account of work sponsored by an agency of the United States Government. Neither the United States Government nor any agency thereof, nor any of their employees, makes any warranty, express or implied, or assumes any legal liability or responsibility for the accuracy, completeness, or usefulness of any information, apparatus, product, or process disclosed, or represents that its use would not infringe privately owned rights. Reference herein to any specific commercial product, process, or service by trade name, trademark, manufacturer, or otherwise, does not necessarily constitute or imply its endorsement, recommendation, or favoring by the United States Government or any agency thereof. The views and opinions of authors expressed herein do not necessarily state or reflect those of the United States Government or any agency thereof.

Metals and Ceramics Division

**EXAMINATION OF BABCOCK AND WILCOX TUBES AFTER EXPOSURE  
IN AN INDUSTRIAL WASTE INCINERATOR**

**J. R. Keiser, M. K. Ferber, H. F. Longmire,  
L.K. Walker, and D. L. Hindman**

**Date Published: June 1996**

**Prepared for the  
Assistant Secretary for Energy Efficiency and Renewable Energy  
Office of Industrial Technologies  
Industrial Energy Efficiency Division and Materials  
for Advanced Industrial Heat Exchanger Program  
ED 21 04 00 0**

**Prepared by the  
OAK RIDGE NATIONAL LABORATORY  
Oak Ridge, Tennessee 37831-6285  
managed by  
LOCKHEED MARTIN ENERGY RESEARCH CORPORATION  
for the  
U.S. DEPARTMENT OF ENERGY  
under contract DE-AC05-96OR22464**

## TABLE OF CONTENTS

LIST OF FIGURES .....	
LIST OF TABLES .....	
ABSTRACT .....	1
1. INTRODUCTION .....	1
2. EXPOSURE CONDITIONS .....	4
3. SAMPLE PREPARATION .....	5
4. RESULTS .....	6
4.1 VISUAL EXAMINATION .....	6
4.2 C-RING STRENGTH MEASUREMENTS .....	6
4.3 MICROSTRUCTURAL EXAMINATION .....	13
4.4 ELECTRON MICROPROBE EXAMINATION .....	35
5. DISUCSSION AND CONCLUSIONS .....	49
6. REFERENCES .....	50
7. ACKNOWLEDGMENTS .....	50

# EXAMINATION OF BABCOCK & WILCOX TUBES AFTER EXPOSURE IN AN INDUSTRIAL WASTE INCINERATOR\*

J. R. Keiser, M. K. Ferber, H. F. Longmire,  
L. R. Walker<sup>†</sup>, and D. L. Hindman<sup>‡</sup>

## ABSTRACT

Seven ceramic tubes provided by, and in most cases manufactured by, Babcock & Wilcox were exposed in E. I. DuPont's Wilmington, Delaware, hazardous waste incinerator. These tubes were subsequently examined at Oak Ridge National Laboratory to determine the effect of exposure on the strength and microstructural integrity of the tube materials. An unexposed tube section of one of the materials was also examined. Evaluation methods included c-ring compression tests, light microscopy, and electron microprobe spectroscopy.

The c-ring compression tests revealed a very wide range in the strengths of the materials tested; the strongest was DuPont Lanxide Composites (DLC) silicon carbide particulate-strengthened alumina, and the weakest was the DLC Type B mixed-oxide material. The only material for which data on unexposed samples were available showed lower strength than the exposed material.

Microstructural examination of the samples yielded minimal evidence of interaction of most of the tube materials with the components of the environment.

Microprobe examination showed some segregation of yttrium in the matrix and along the surface of one of the PRD166/zirconia tubes and limited interaction of the fibers in the same tube with the components of the environment.

---

## 1. INTRODUCTION

Examinations of samples exposed in the earlier stages of this study have been described in previous publications.<sup>1-3</sup> Information provided by Babcock & Wilcox (B&W) for the tubes examined in this study is shown in Table 1. The seven exposed tubes sent to Oak Ridge National Laboratory (ORNL) were approximately 1.52 m (5 ft) long and 10.2 cm (4 in.) in

---

\*Research sponsored by the U.S. Department of Energy, Assistant Secretary for Energy Efficiency and Renewable Energy, Office of Industrial Technologies, Industrial Energy Efficiency Division and Materials for Advanced Industrial Heat Exchanger Program, under contract DE-AC05-96OR22464 with Lockheed Martin Energy Research Corp.

<sup>†</sup>Lockheed Martin Energy Systems, Analytical Services Division, Oak Ridge Y-12 Plant, Oak Ridge, TN 37831

<sup>‡</sup>Babcock & Wilcox, Lynchburg Research Center, Lynchburg, VA 24506

Table 1. Characteristics of tubes examined

Tube Identif.	Exposure position	Observations	Materials	Exposure period
1	Right side, front row	Helically wound fibers	Nextel 610 fibers zirconia matrix	8 weeks
3	Center of center row	Hoop-wound fibers on surfaces, helically wound internal fibers, thermocouples on tube	Almax fibers zirconia matrix	27 weeks
4	Center of rear row	Hoop-wound fibers on surfaces, helically wound internal fibers, some unbonded layers	PRD166 fibers zirconia matrix	27 weeks
5	Left side, rear row	Hoop-wound fibers on surfaces, helically wound internal fibers, some unbonded layers	PRD166 fibers zirconia matrix	27 weeks
6	Right side, center row	No evidence of fibers, ~ 0.25 in. thick	SiC particles alumina matrix	27 weeks
7	Right side, rear row	Appears to be helically wound fibers, ~ 0.375 in. repeat	Type B mixed oxides	8 weeks
9	Left side, center row	Appears to be helically wound fibers, ~ 0.375 in. repeat	Type B mixed oxides	8 weeks
AR	Unexposed	Hoop-wound fibers, some unbonded layers	PRD166 fibers zirconia matrix	None

outside diameter. There was a considerable difference in the wall thickness of the tubes; the thinnest wall was < 3.2 mm (0.125 in.) thick while the thickest was about 6.4 mm (0.25 in.) thick.

All tubes that were exposed in the incinerator were closed at one end and were flared or had a flange at the other end. In order to expedite the examination, no photographs were taken of the tubes when they were received at ORNL, but they all had some surface deposits ranging in color from tan to light grey that were presumed to have resulted from deposition during exposure in the incinerator. The exposed tubes are shown in Fig. 1 after removal of a section from near the bottom of each tube to provide samples. The unexposed tube section that was supplied later is shown in Fig. 2.

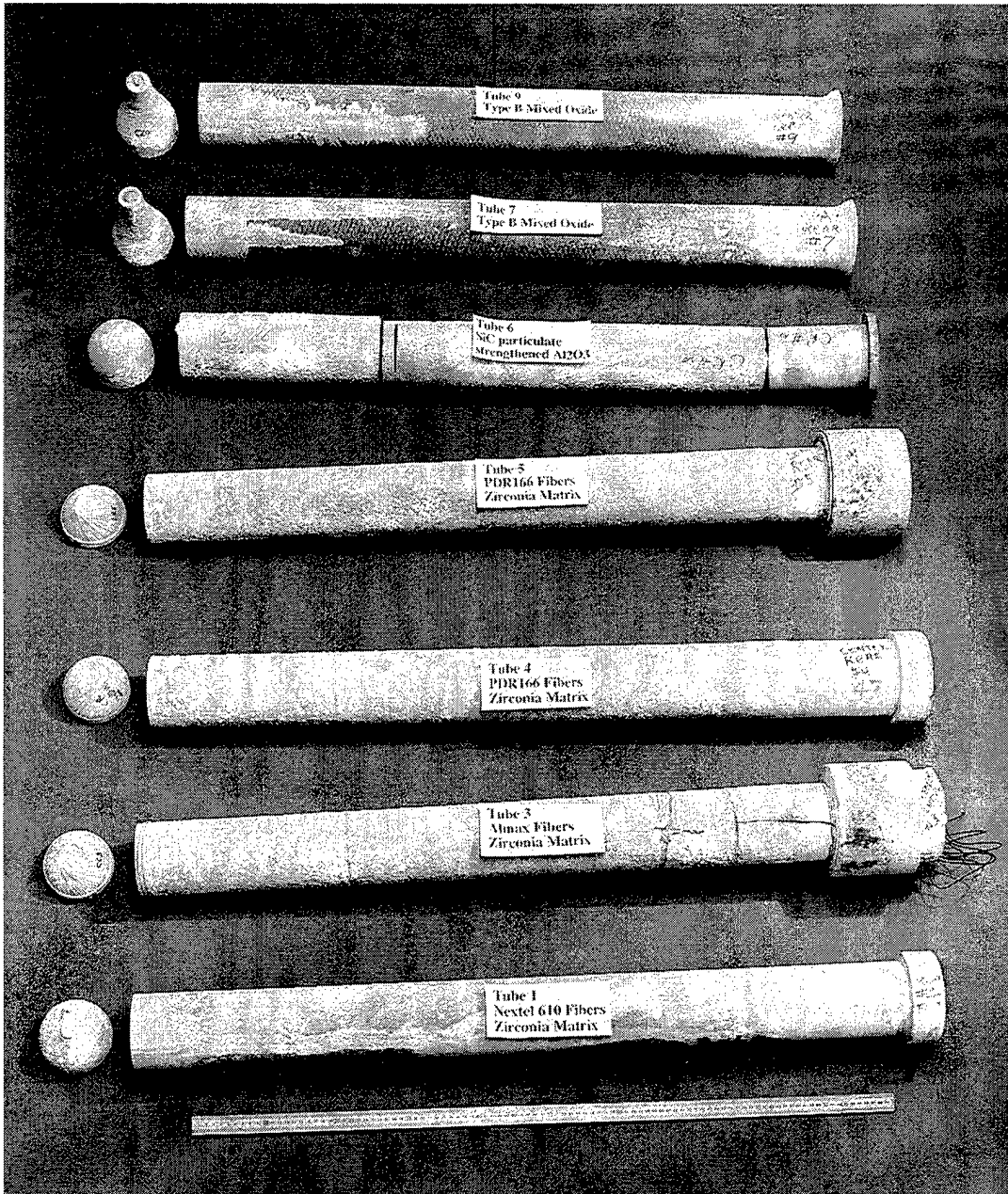


Fig. 1. Tubes exposed in DuPont hazardous waste incinerator. Sections used for c-ring samples have been cut from near the closed end of the tubes.

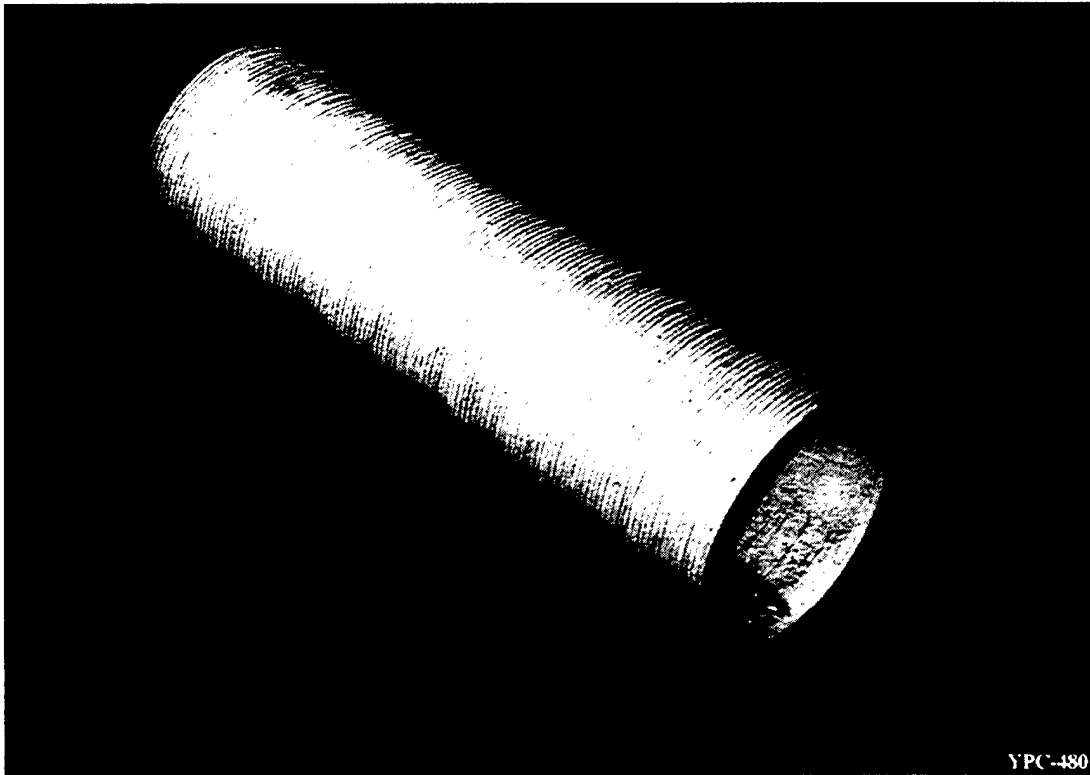


Fig. 2. Unexposed piece of PRD166/zirconia tubing used as reference material in examination.

## 2. EXPOSURE CONDITIONS

The ceramic tubes were exposed in a module that was added upstream of the incinerator's spray dryer (quench chamber) such that a portion of the incinerator effluent gas could be routed through this module. Tubes were positioned in the heat exchanger module in a 3 by 3 array. Unfortunately, exposure of the tubes in this slipstream configuration met with a number of problems. Backflowing of steam into the tubes was thought to be the cause of failure for a number of the tubes. Because of the operating difficulties encountered, a number of the tubes had to be replaced so that not all the tubes had the same exposure time. The original tube installation occurred on April 20, 1994; the tubes that survived for the entire test were removed February 3, 1995, and had approximately 27 weeks of exposure under incinerator conditions. Three tubes were installed on November 30, 1994, and these tubes received approximately 8 weeks of actual incinerator exposure.

In a typical week, the incinerator was in operation for about 105 h, from about 3 p.m. Monday until around midnight Friday. The flue gas exiting the afterburner was about 954°C (1750°F) at a point that was about 6.1 m (20 ft) away from the heat exchanger tubes. The maximum flue gas temperature measured inside the heat exchanger was reported to be 899°C (1650°F). During a typical day of operation, there would usually be at least two burndown cycles; the incinerator was allowed to cool to about 260°C (500°F) to allow maintenance to be done. Frequent temperature fluctuations over a day's operation created additional stresses on the tubes.

### 3. SAMPLE PREPARATION

The tubes were delivered to ORNL in approximately the same condition as when removed from the incinerator. Tube surfaces were covered with a powdery deposit, and the thermocouples (TCs) were still attached to the tube that had been in the center of the tube array. As a precaution, the tubes were generally handled with gloves, and all cutting was done with the tubes wet to prevent production of a possibly hazardous dust. The preparation of samples began with the removal of an approximately 35.6-cm (14-in.)-long piece from near the bottom of each tube. Each of these pieces was cut into rings from which c-ring samples were prepared. C-rings were nominally 17.8 mm (0.7 in.) wide except for two samples, each 5.08 mm (2 in.) wide, that were cut from the Nextel 610/zirconia tube. The wider samples were used because the repeat distance on the weave was approximately 5 cm, and the tube wall was considerably thinner than for all of the other tubes examined.

The smaller sections cut from the rings were submitted for microstructural examination. These small sections were mounted in epoxy so that the cross section could be viewed; both longitudinal and transverse sections were prepared for each tube. The inner and outer surfaces, as well as an area near the center of every sample, were examined. The electron microprobe was used to search for evidence of interaction of the remnants of the incinerated material with the ceramic tube constituents.

Sections 101.6 mm (4 in.) in length were also cut from each tube and sent to Argonne National Laboratory for thermal conductivity measurements. Results of these measurements are not included in this report.

## 4. RESULTS

### 4.1 VISUAL EXAMINATION

During the preparation of the c-ring samples, it was evident that a lack of cohesion existed between some of the fiber layers. This lack of bonding was evident during the microstructural examination and is shown on micrographs taken near the center of some of the samples. The untested c-rings were visually examined to identify any significant features. Tube 1 showed a regular repeating pattern in the woven structure of the helically wrapped ceramic fibers. Tubes 3, 4, and 5 had a middle layer of low-angle ( $\pm 15^\circ$ ) helically wound fibers with inner and outer layers of hoop-wrapped fiber that did not show the repeating pattern of several of the other tubes. Tube 6 showed no evidence of fibers; the relatively thick wall and the surface layers were characteristic of DuPont Lanxide Composites (DLC) silicon carbide particulate-strengthened alumina. Tubes 7 and 9 appeared to be helically wound ceramic fiber composite tubes, but conversations with a manufacturer's representative<sup>4</sup> indicated the original fibers had been intentionally degraded by thermal processing, leaving a structure that had the appearance of fibers but none of the structural attributes of a ceramic fiber composite.

Most of the surfaces of the tubes that had been exposed to the incinerator environment had rough, loosely adhering surface deposits. There was no visible evidence of matrix or fiber damage, but some delamination or lack of internal bonding was apparent for the PRD166/zirconia samples and the Almax/zirconia samples.

### 4.2 C-RING STRENGTH MEASUREMENTS

The c-ring samples were compression tested at room temperature in a commercially available, twin-screw, electromechanical test machine (manufactured by Applied Test Systems, Butler, Pennsylvania) using a cross-head speed of 0.02 in./min. At least four samples of each material were tested. The test system is shown in Fig. 3, and a sample being tested in the system is shown in Fig. 4. For this configuration, the maximum tensile stress is developed at the midspan of the outer surface. The expression used to relate compressive load to this maximum stress<sup>5</sup> is strictly valid for linear elastic, isotropic materials. For the fiber-reinforced materials examined in this study, the reported strength values should be used for comparative purposes only. In fact, the factors affecting the validity of flexure tests of continuous fiber-reinforced composites apply to the case of the compressively loaded c-ring.

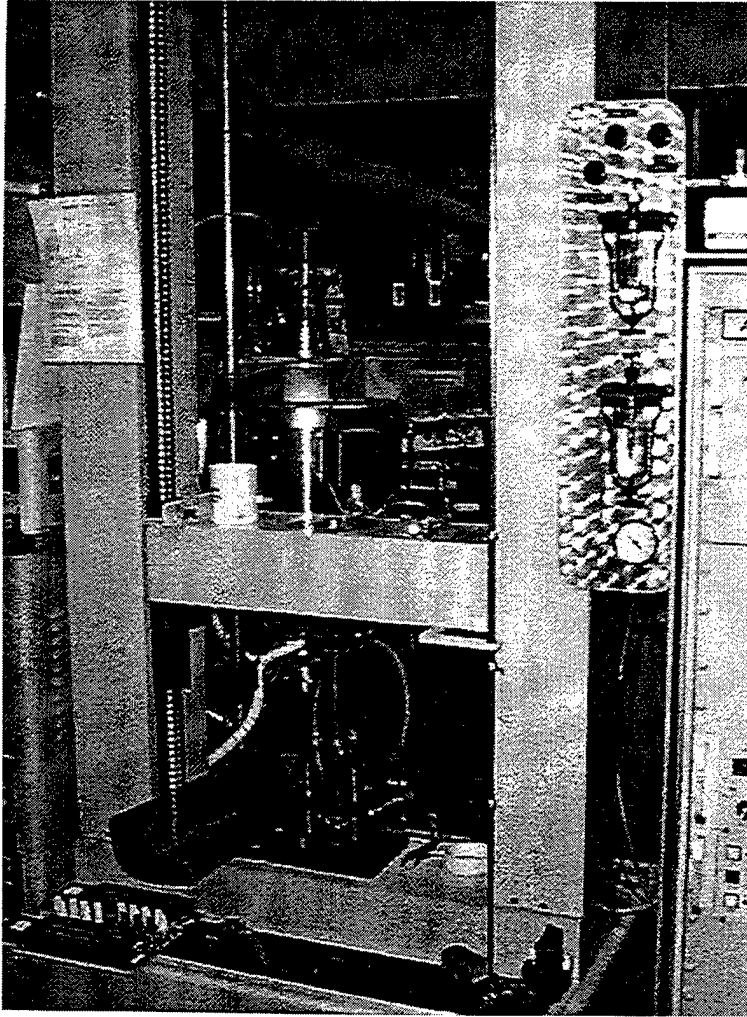


**Fig. 3.** Twin-screw electromechanical test machine used for room-temperature c-ring tests.

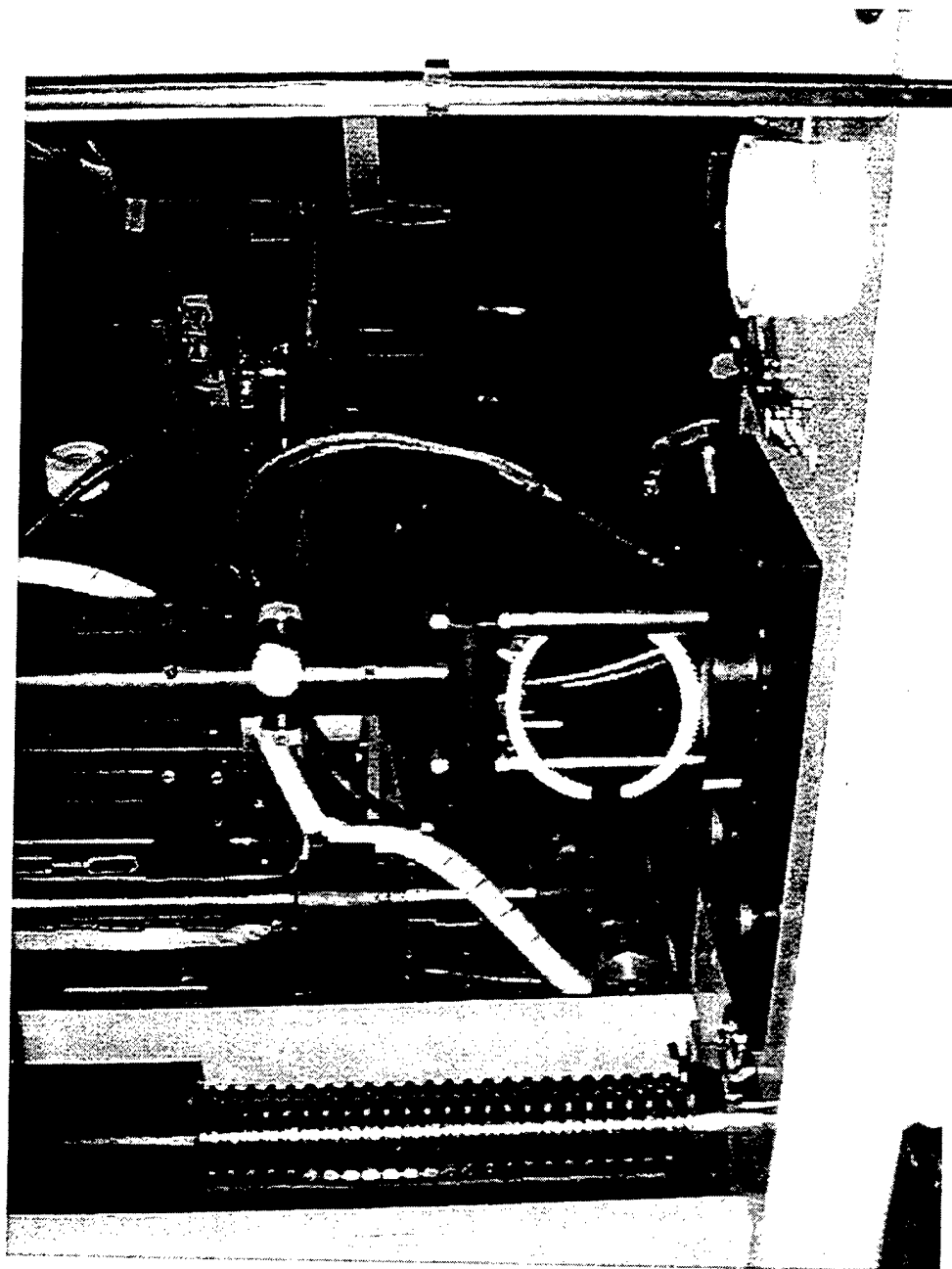


Fig. 4. C-ring sample being compression tested in electromechanical test machine.

The results of all the compression tests are summarized in Table 2, where the results for each individual test are given along with the average and the standard deviation. A graphical comparison of these results is given in Fig. 5, which shows that tube 6 was by far the strongest; it demonstrated a strength more than twice that of all other materials tested.

For tube 1, two samples were prepared and tested with the standard 17.8 mm width while two others were fabricated to be approximately 50 mm wide. The loading curves for all four of the tests are shown in Fig. 6. No effect of sample width on the maximum strength was seen, and, in fact, the standard deviation was the smallest for all the materials tested. This material combination was the weakest of the ceramic fiber-ceramic matrix composite materials, and this weakness is most likely due to the fiber architecture that contains helically wrapped, but no hoop-wrapped, fibers.

Five samples from tube 3 were tested, and the variation in strength was relatively limited, especially considering the apparent presence of incomplete bonding in the tube wall. Depending on the orientation of the unbonded areas during compression testing, significant strength reductions can result. The loading curves for the five samples are shown in Fig. 7.

**Table 2. Results of c-ring compression tests**

Tube identification	Strength (MPa)	Standard deviation	Measured strengths (MPa)
1	25.59	3.04	24.11, 27.86, 28.37, and 22.04
3	68.12	10.54	68.74, 58.04, 56.85, 79.06, and 77.92
4	101.40	20.28	128.58, 97.60, 82.45, 115.35, and 83.01
5	82.89	12.79	67.27, 95.93, 90.25, and 78.09
6	278.41	51.35	202.89, 247.07, 318.86, 308.52, and 314.71
7	21.61	3.21	16.99, 23.15, 22.00, and 24.28
9	18.46	7.10	7.94, 21.87, 20.69, and 23.34
AR	62.60	14.83	71.15, 64.60, 73.55, and 41.10

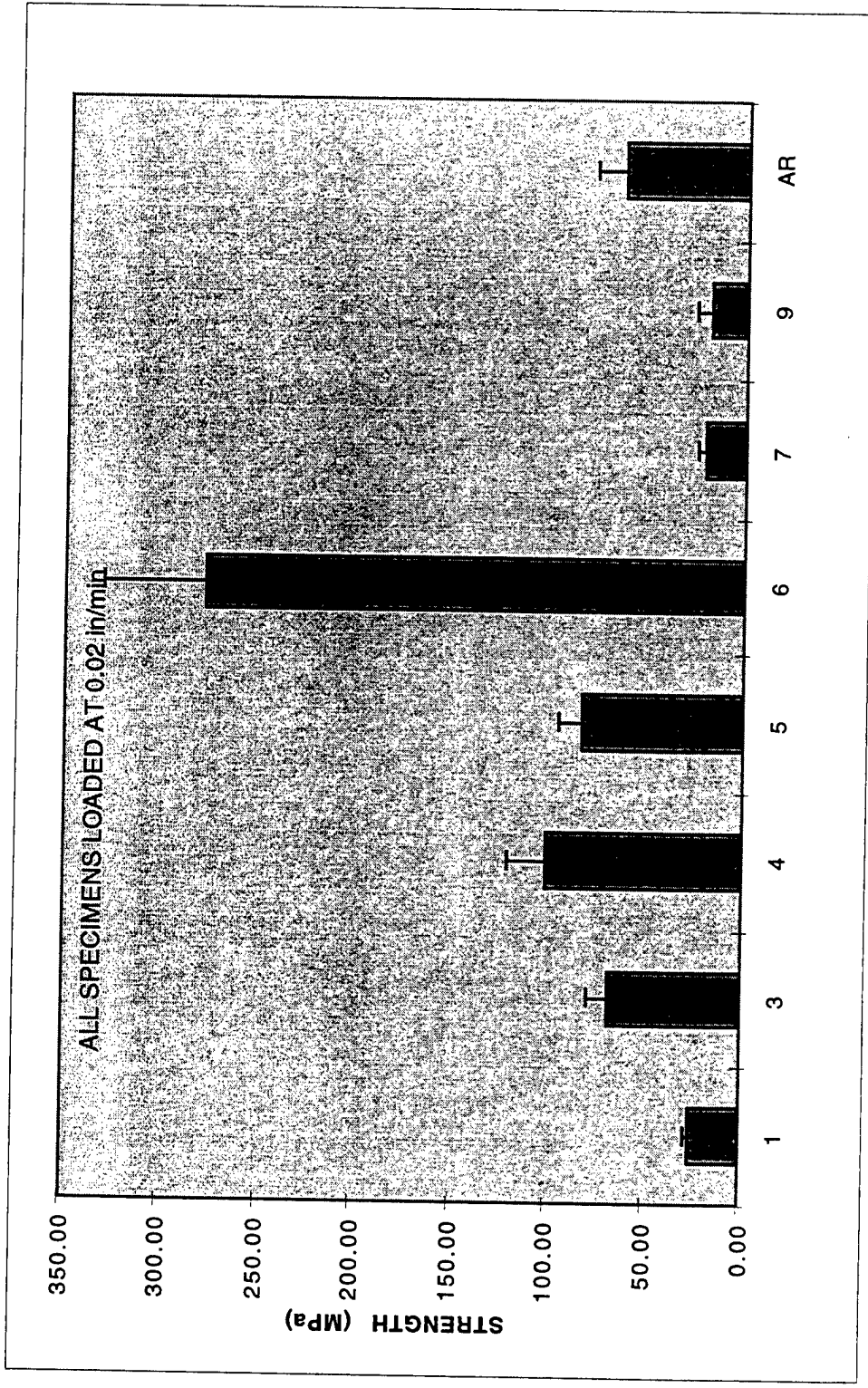


Fig. 5. Average strengths and standard deviations calculated from c-ring compression tests of ceramic composite materials exposed in industrial waste incinerator.

TUBE 1

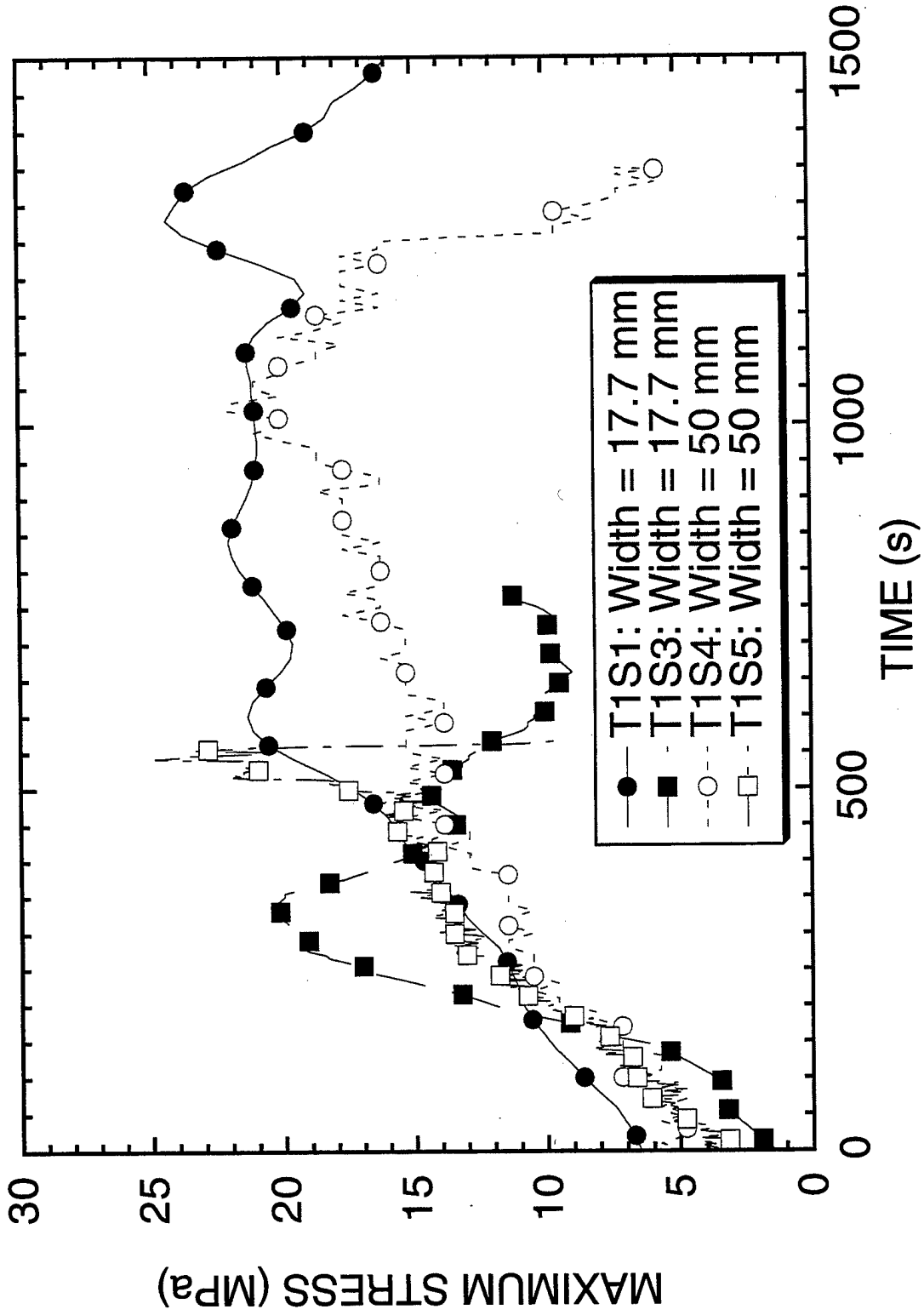


Fig. 6. Loading curves for c-ring compression tests conducted on Nextel 610/zirconia tube (Babcock & Wilcox designation-tube 1).

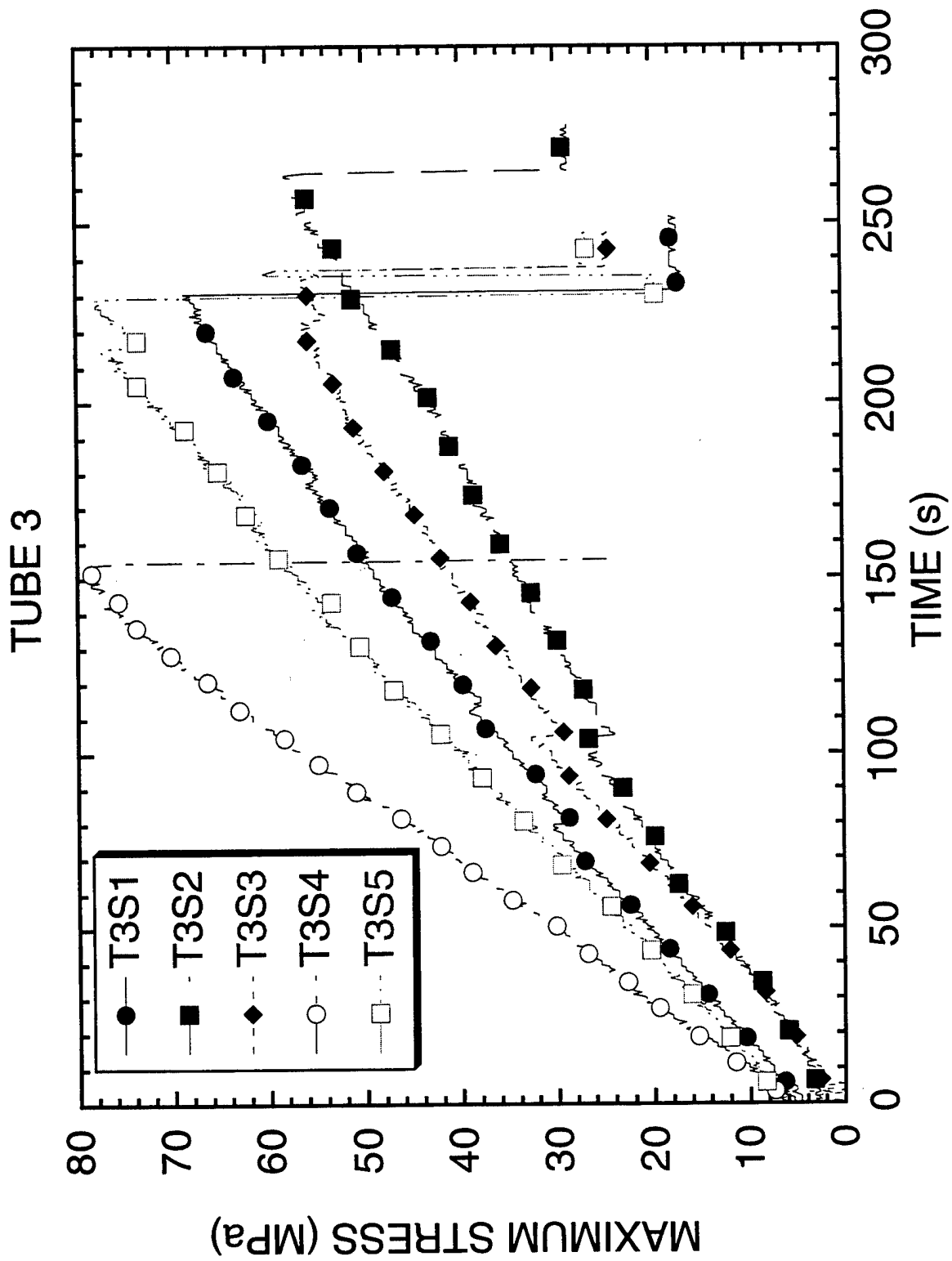


Fig. 7. Loading curves for c-ring compression tests conducted on Almax/zirconia tube (Babcock & Wilcox designation-tube 3).

Tubes 4 and 5 were constructed of the same material, and five and four samples, respectively, were tested. Loading curves for the two tubes are shown in Figs. 8 and 9. These curves show that two samples from tube 4 were significantly stronger than the other samples of this material while tube 5 had one sample that was noticeably weaker than the other samples of this material. Although there was appreciable variation in the measured strengths, this material was the second strongest of all materials tested and the strongest of the ceramic fiber/ceramic matrix combinations tested.

The strongest material in these tests was the particulate-strengthened material used for tube 6. Five samples were tested and the loading curves are shown in Fig. 10. Two of these samples failed at loads considerably lower than the failure loads for the other three samples, and this accounted for the relatively large standard deviation for this material.

The weakest material tested was that used for tubes 7 and 9, and results of the c-ring compression tests are shown in Figs. 11 and 12. Four samples of each tube were tested, and one sample was considerably weaker than the other seven. Although this material had the appearance of a ceramic fiber/ceramic matrix composite, the thermal treatment given the tubes resulted in a highly microcracked structure that had high thermal shock resistance but low strength.<sup>4</sup>

C-rings from an unexposed tube of the same material as tubes 4 and 5 were tested, and the loading curves from these tests are shown in Fig. 13. One of these c-rings was considerably weaker than the other three; however, all of these c-rings were weaker than seven of the eight exposed samples that were tested.

### 4.3 MICROSTRUCTURAL EXAMINATION

As noted earlier, the small pieces cut from the rings were submitted for microstructural examination. The examinations concentrated on the outer surface of each sample, but a region near the center of each sample, as well as the inner surface of each sample, was also inspected. Micrographs of the outer surface of a sample from each tube are shown in Figs. 14 through 20 along with a micrograph of the center of each sample.

Micrographs of the Nextel 610/zirconia sample shown in Fig. 14 show some porosity a short distance below the surface. From the higher magnification picture, there is no evidence that the fibers at and near the surface were degraded by any reaction with the environment. The micrograph taken near the center of the sample also shows some porosity in this sample.

The Almax/zirconia sample is shown in Fig. 15, and, as with the Nextel/zirconia, there is no evidence of a reaction of the fibers near the surface of the sample with the components of

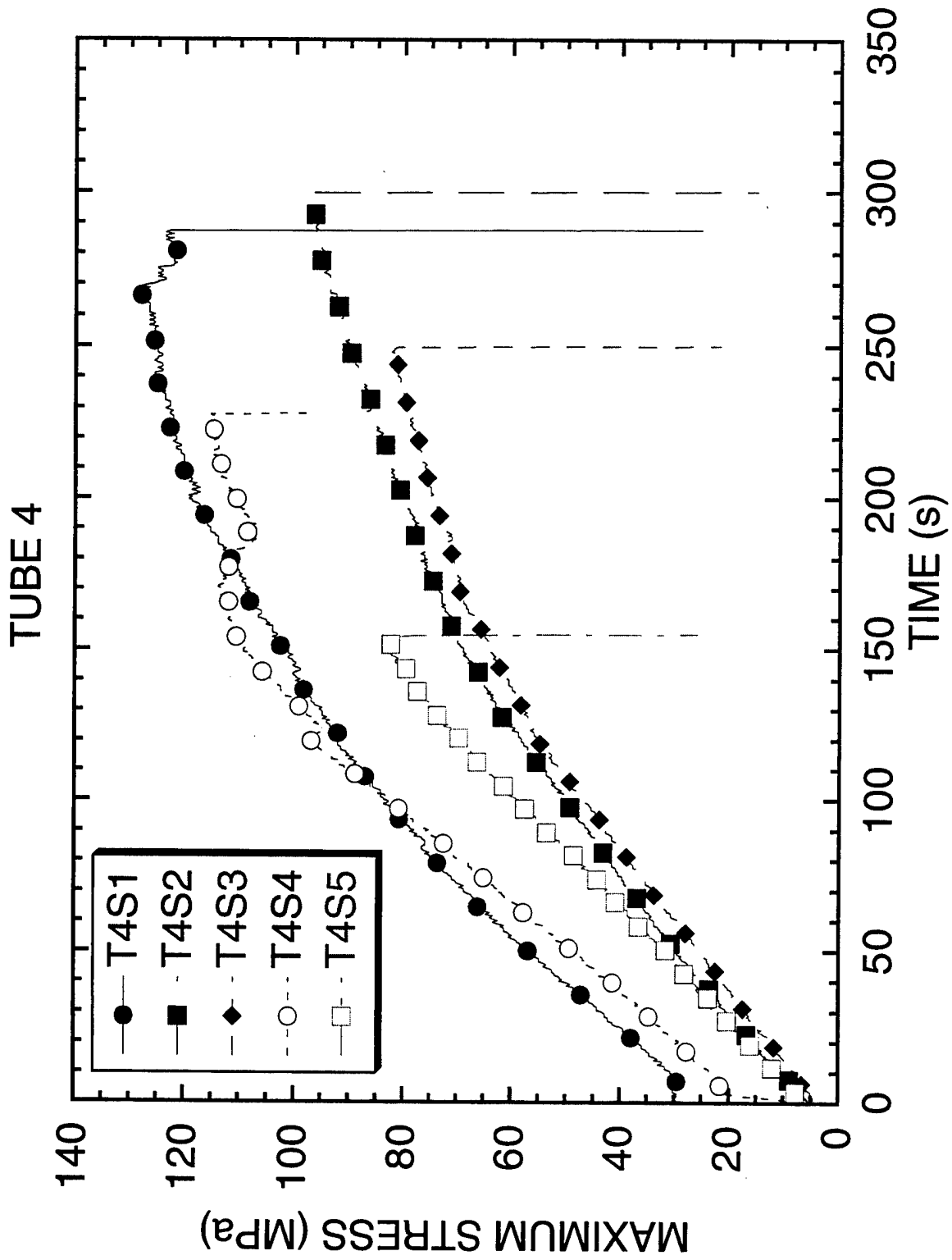


Fig. 8. Loading curves for c-ring compression tests conducted on PRD166/zirconia tube (Babcock & Wilcox designation-tube 4).

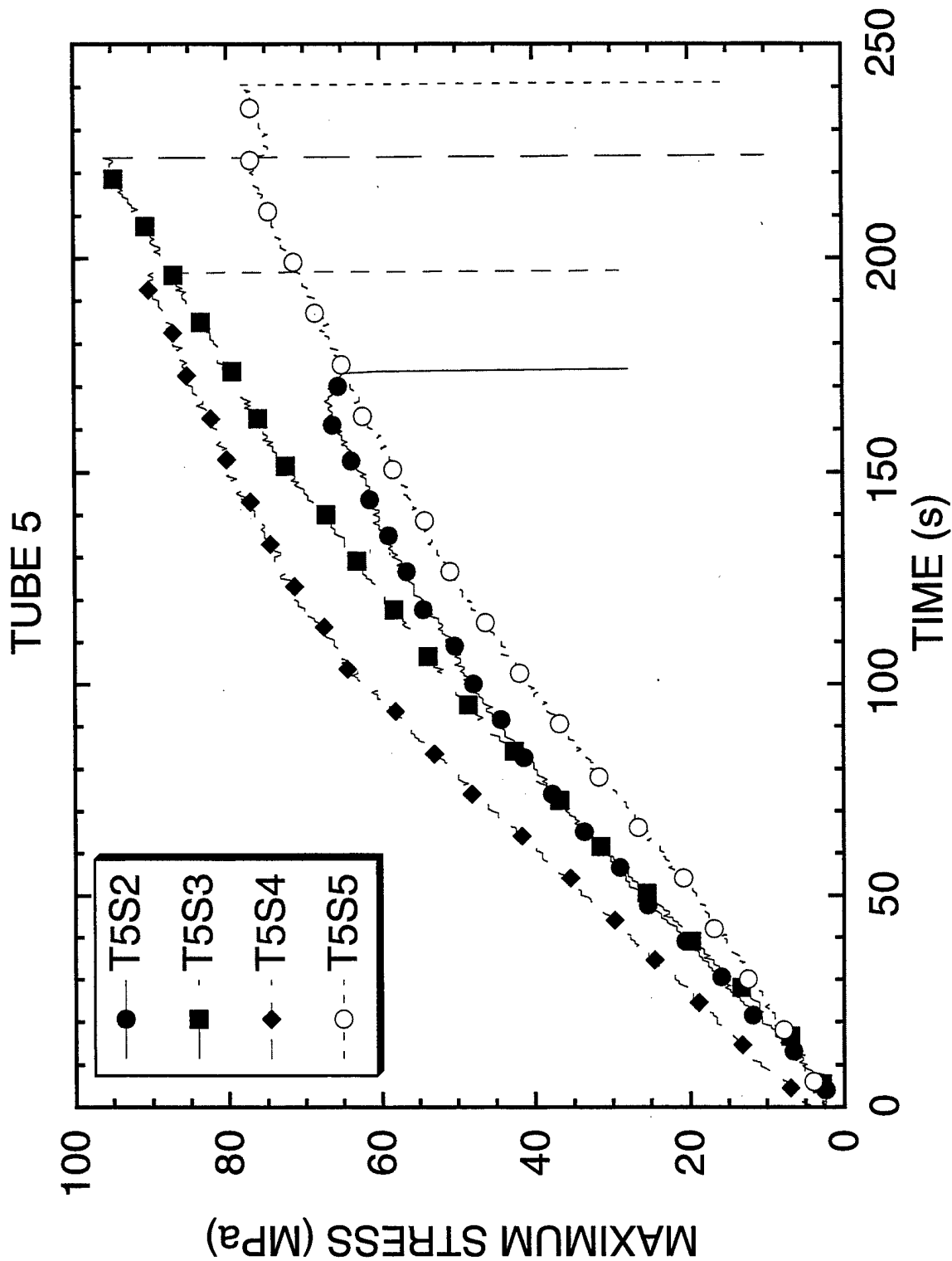


Fig. 9. Loading curves for c-ring compression tests conducted on PRD166/zirconia tube (Babcock & Wilcox designation-tube 5).

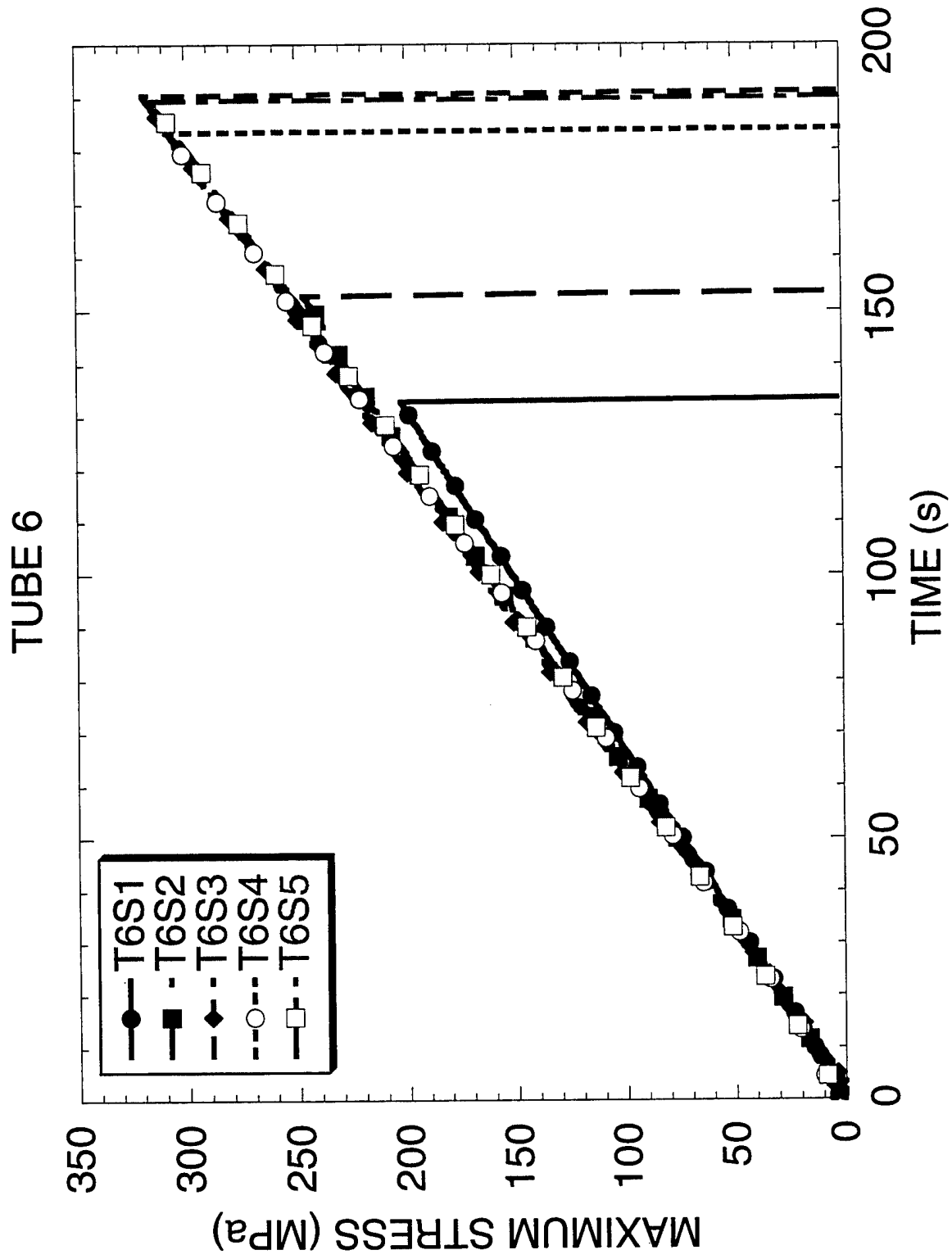


Fig. 10. Loading curves for c-ring compression tests conducted on  $\text{SiC-Al}_2\text{O}_3$  tube (Babcock & Wilcox designation-tube 6).

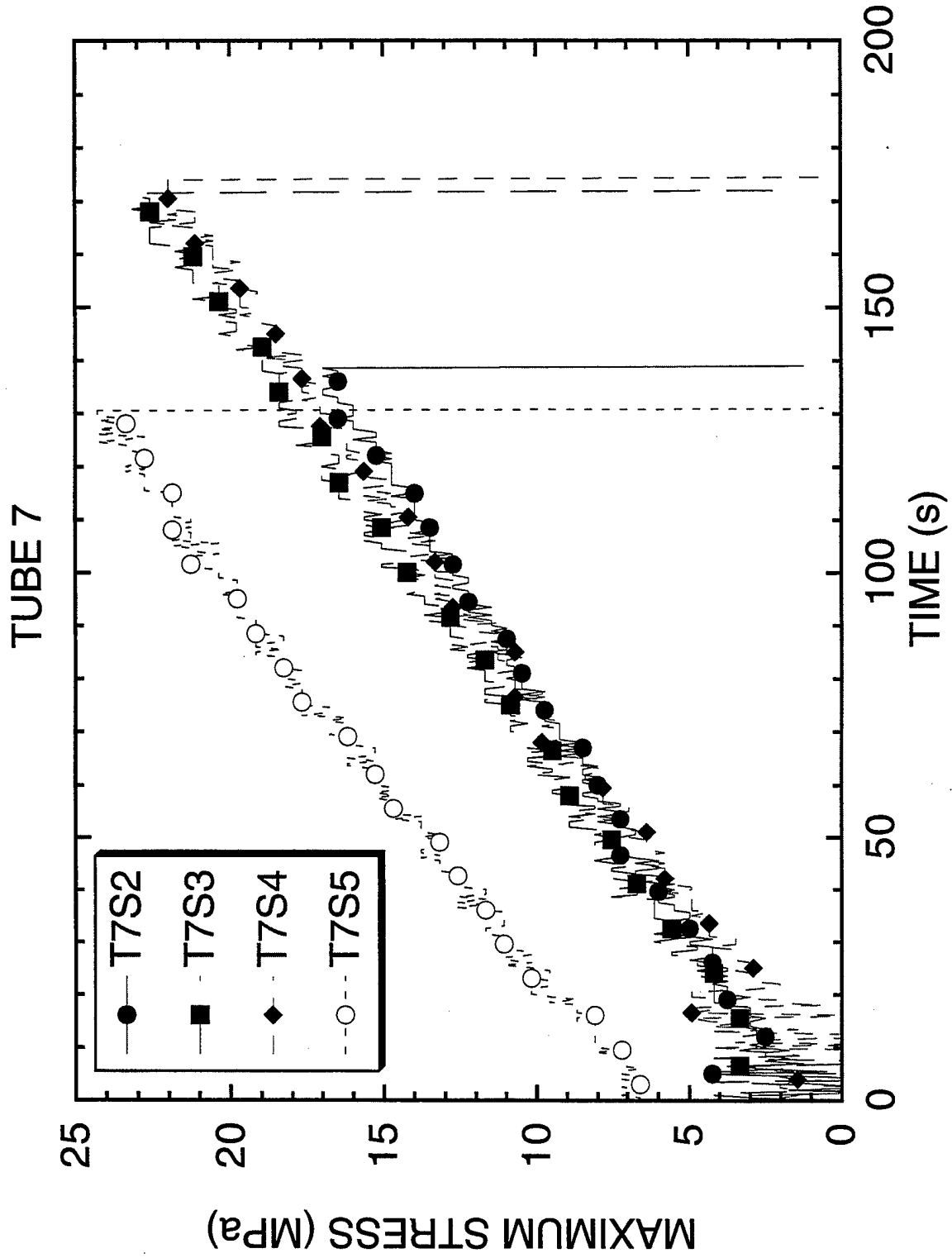


Fig. 11. Loading curves for c-ring compression tests conducted on mixed-oxide tube (Babcock & Wilcox designation-tube 7).

# TUBE 9

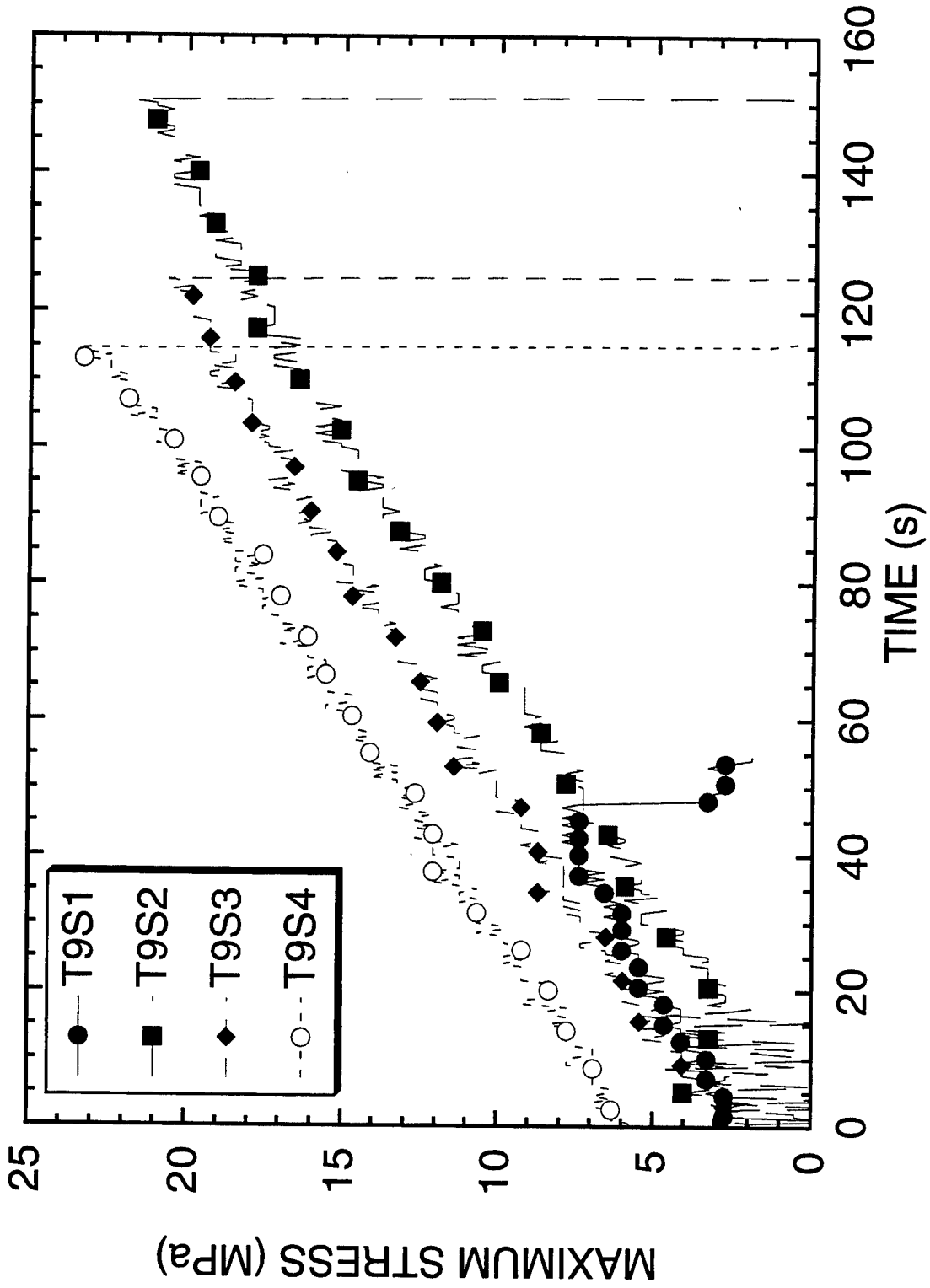


Fig. 12. Loading curves for c-ring compression tests conducted on mixed-oxide tube (Babcock & Wilcox designation-tube 9).

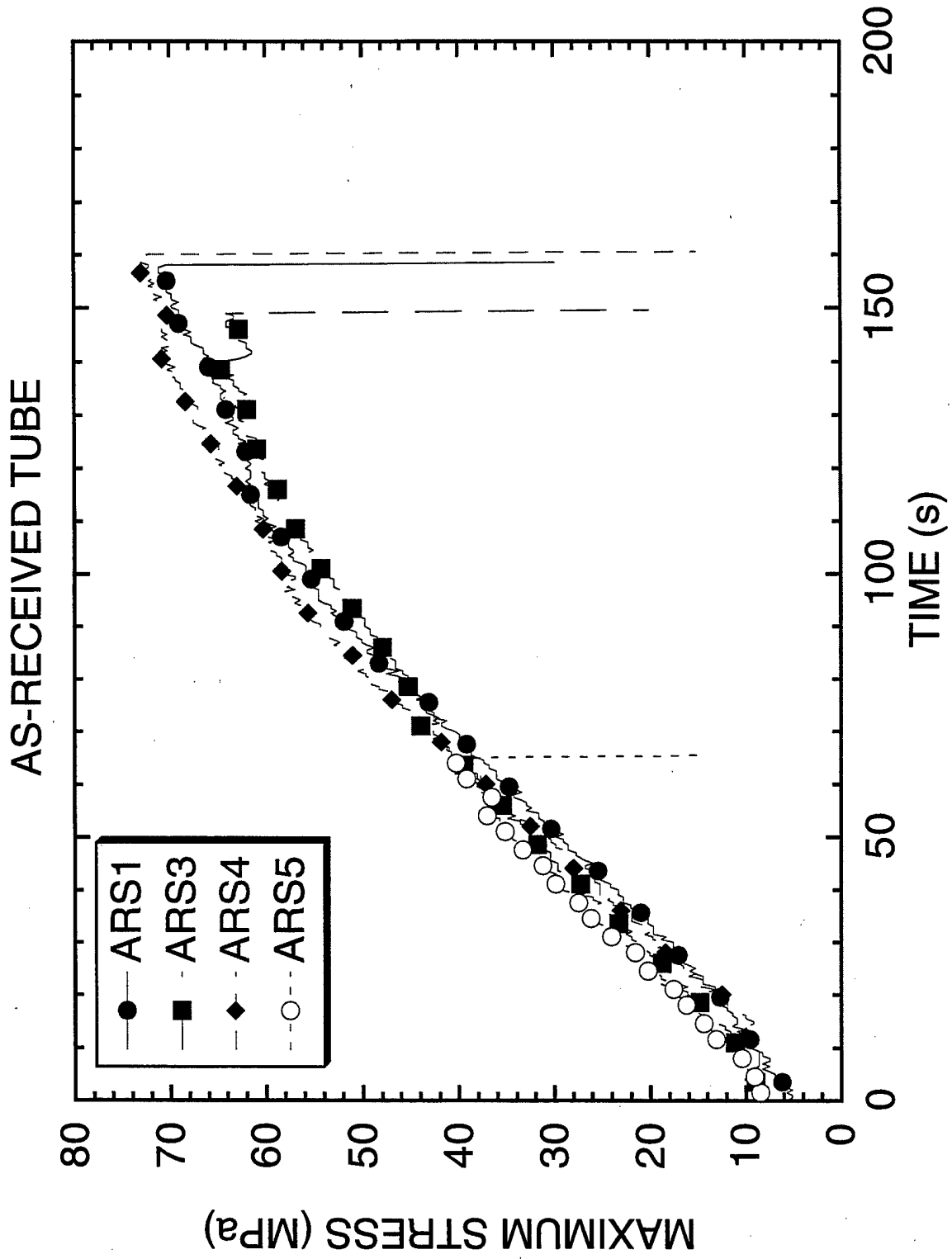


Fig. 13. Loading curves for c-ring compression tests conducted on unexposed PRD166/zirconia tube (Babcock & Wilcox designation-tube AR).

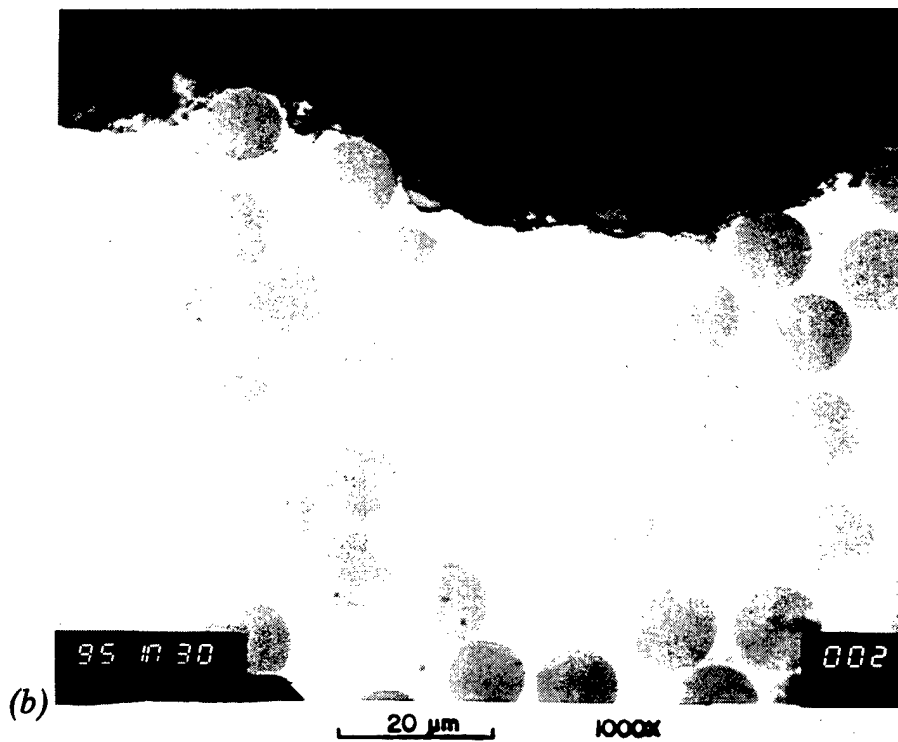
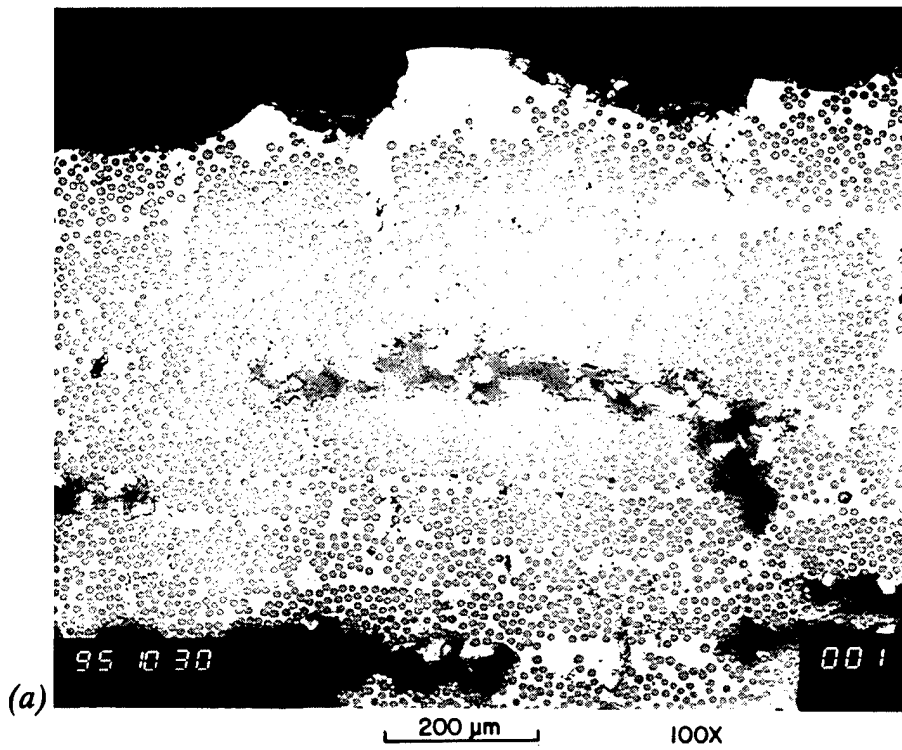
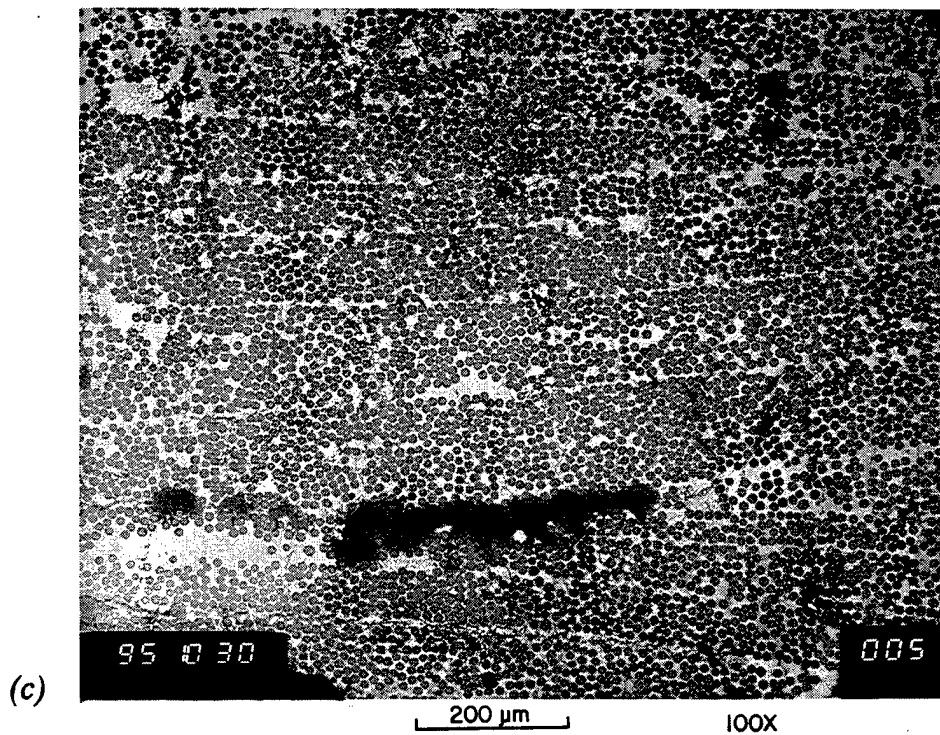


Fig. 14. Photomicrographs at (a) low and (b) high magnification of the tube's outer surface and (c) an area near the center of the Nextel 610/zirconia sample.



**Fig. 14 (continued).** Photomicrographs at (a) low and (b) high magnification of the tube's outer surface and (c) an area near the center of the Nextel 610/zirconia sample.

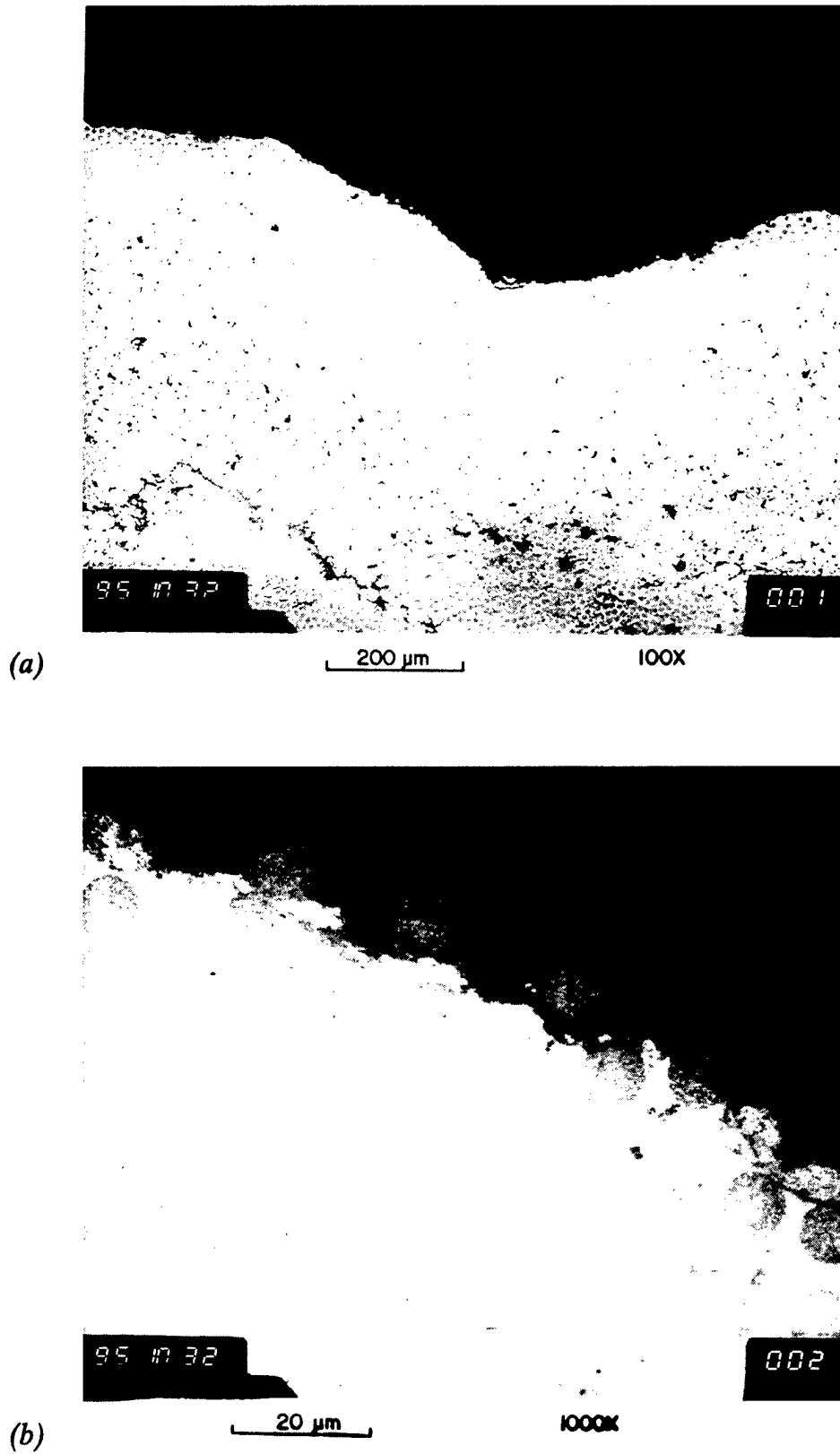
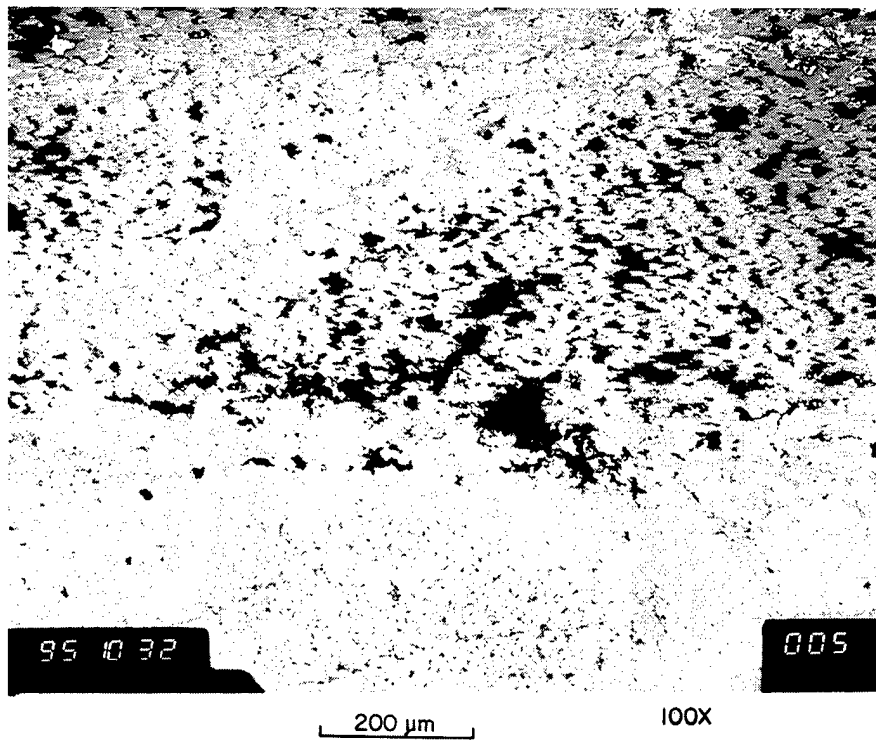


Fig. 15. Photomicrographs at (a) low and (b) high magnification of the outer surface and (c) an area near the center of the wall of the Almax/zirconia sample (tube 3).



**Fig. 15** (continued). Photomicrographs at (a) low and (b) high magnification of the outer surface and (c) an area near the center of the wall of the Almax/zirconia sample (tube 3).

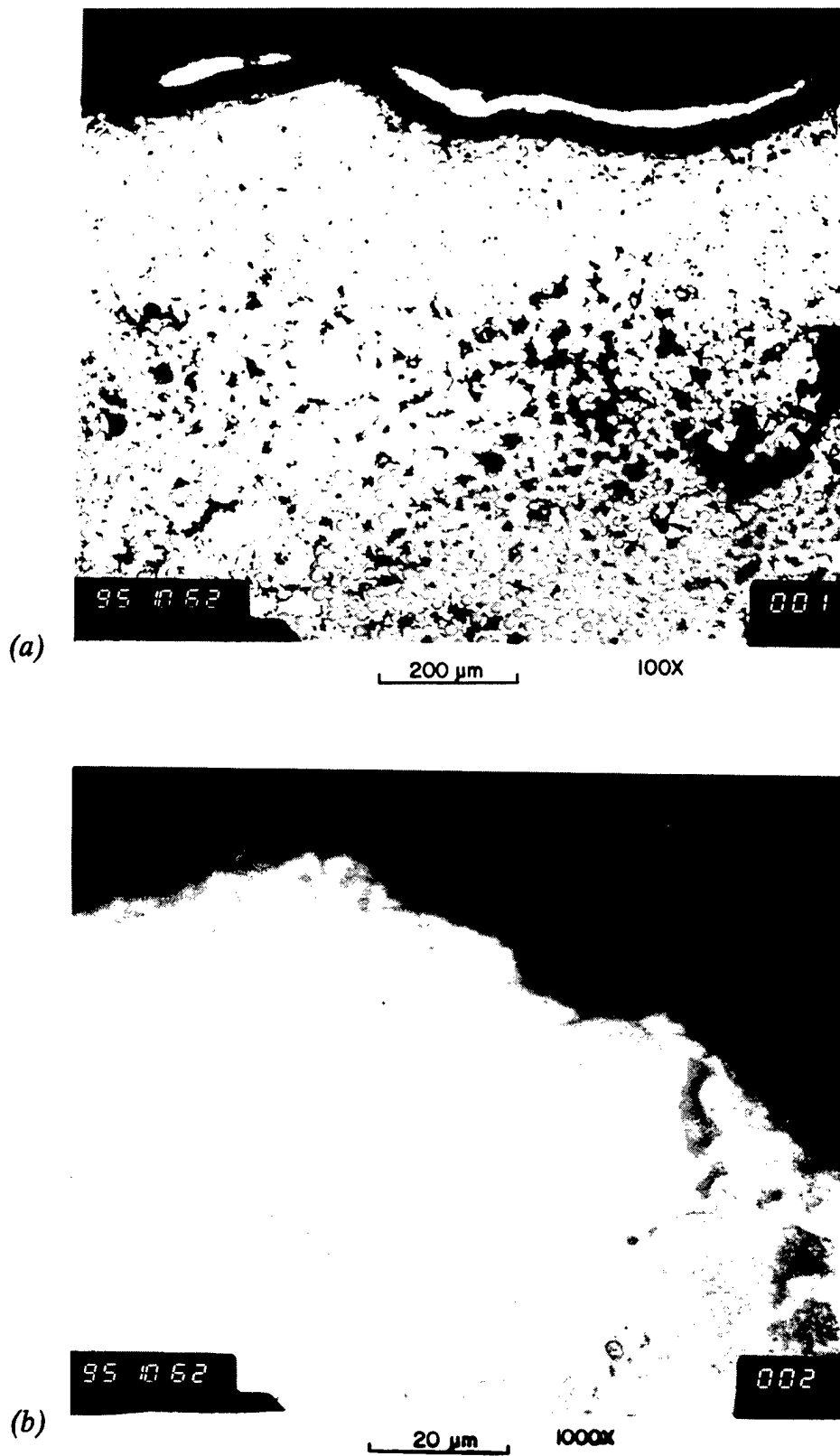
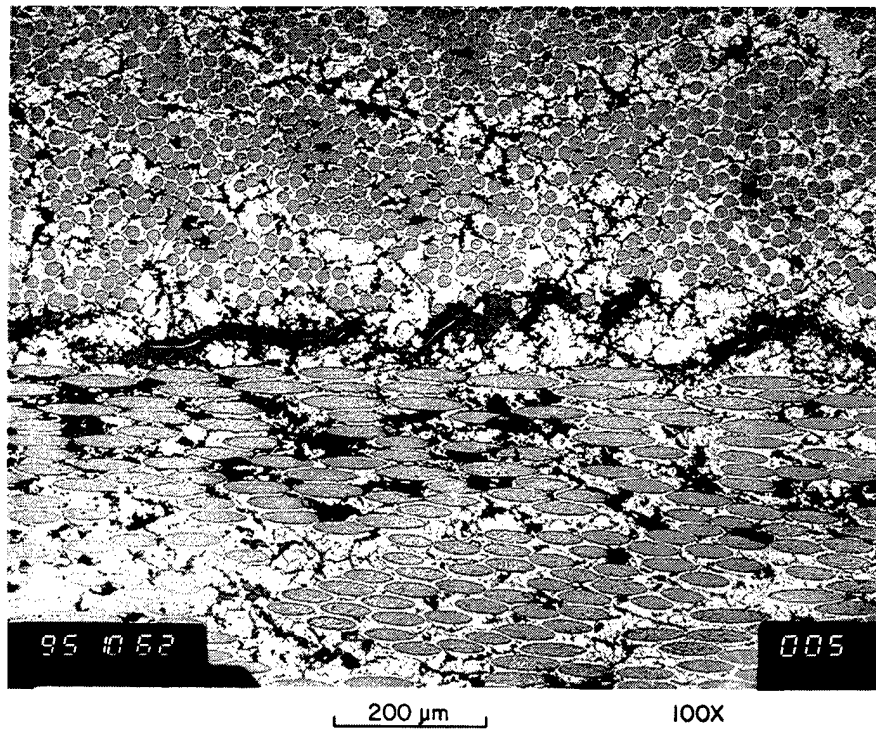


Fig. 16. Photomicrographs at (a) low and (b) high magnification of the tube's outer surface and (c) an area near the center of the wall of the PRD166/zirconia tube (tube 4).



(c) Fig. 16 (continued). Photomicrographs at (a) low and (b) high magnification of the tube's outer surface and (c) an area near the center of the wall of the PRD166/zirconia tube (tube 4).

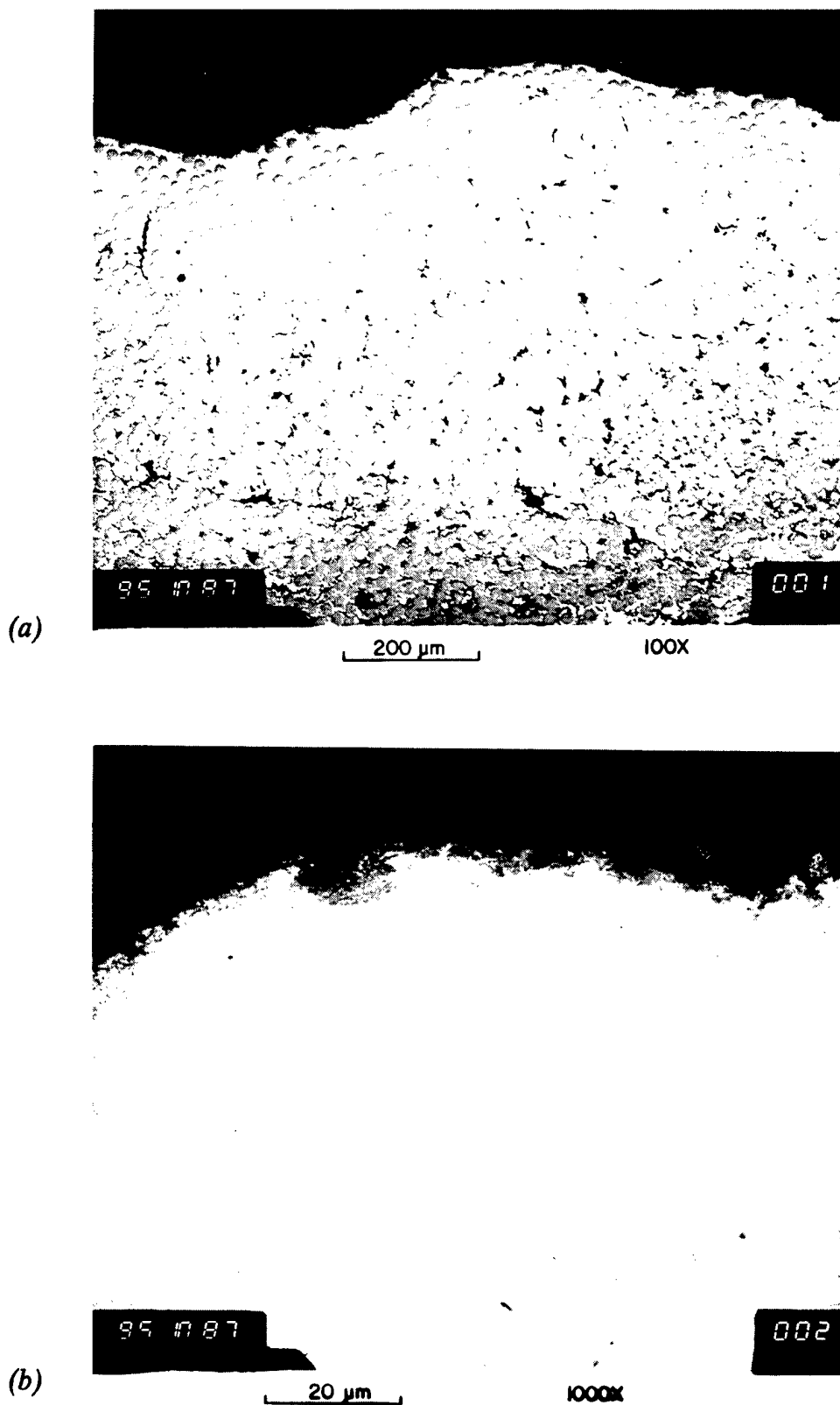
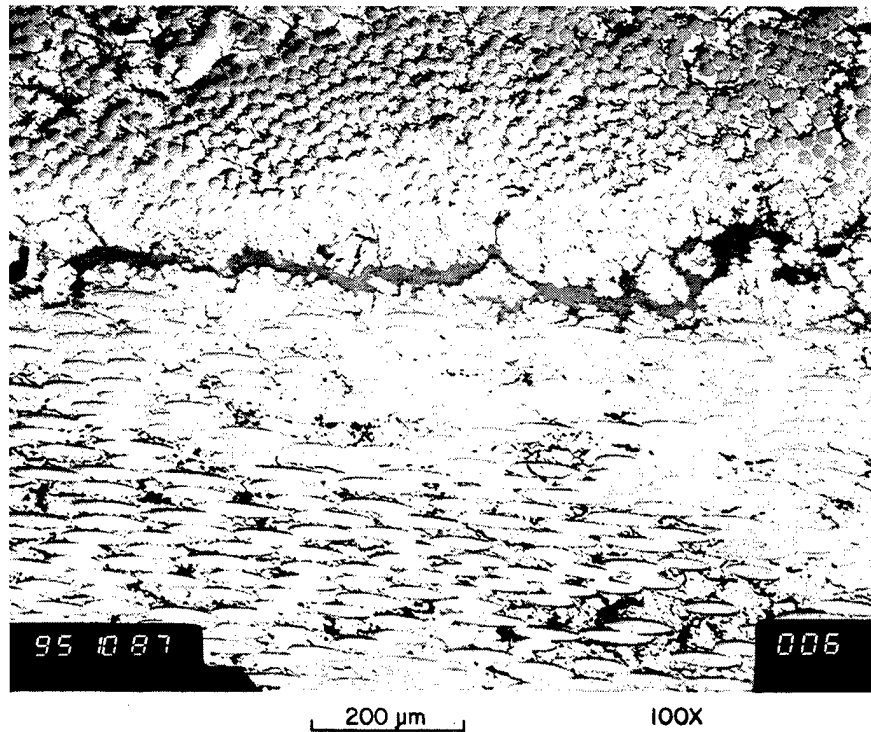


Fig. 17. Photomicrographs at (a) low and (b) high magnification of the tube's outer surface and (c) an area near the center of the wall of the PRD166/zirconia tube (tube 5).



(c)  
Fig. 17 (continued). Photomicrographs at (a) low and (b) high magnification of the tube's outer surface and (c) an area near the center of the wall of the PRD166/zirconia tube (tube 5).

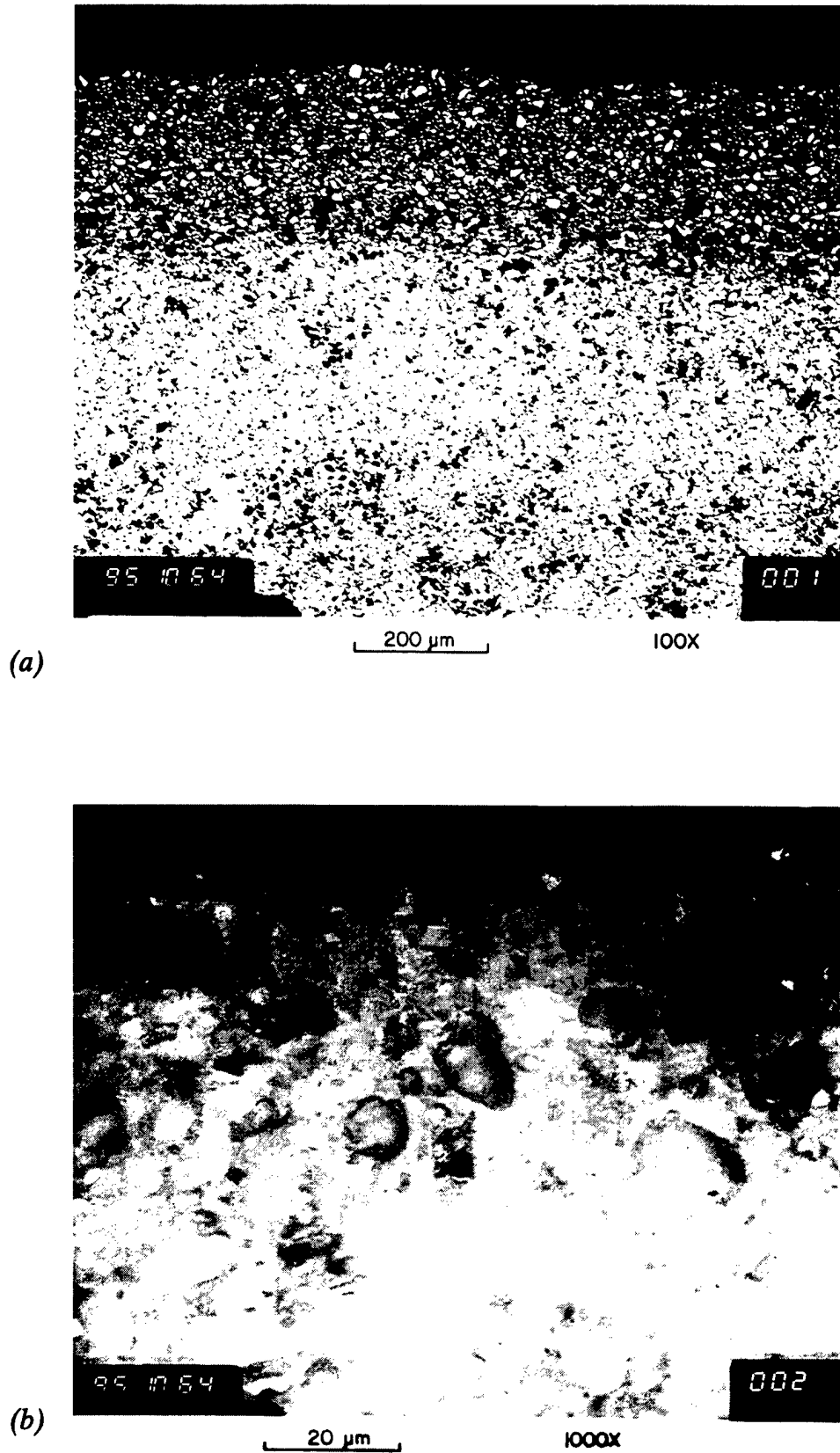


Fig 18. Photomicrographs at (a) low and (b) high magnification of the tube's outer surface and (c) an area a short distance below the outer surface of the  $\text{SiC}_p\text{-Al}_2\text{O}_3$  tube.

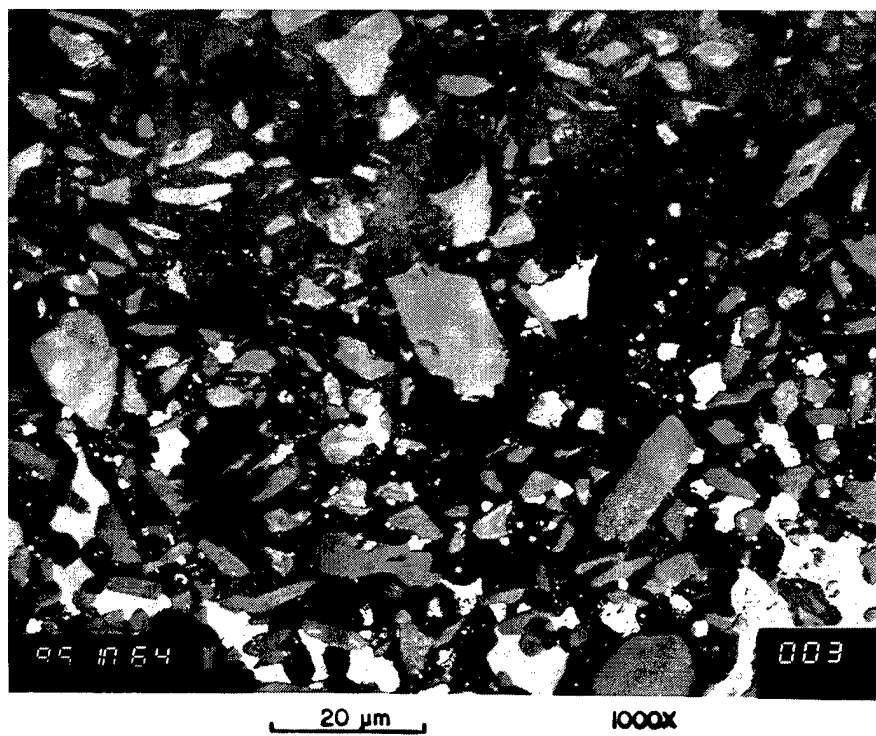


Fig. 18 (continued). Photomicrographs at (a) low and (b) high magnification of the tube's outer surface and (c) an area a short below the outer surface of the  $\text{SiC}_p\text{-Al}_2\text{O}_3$  tube.

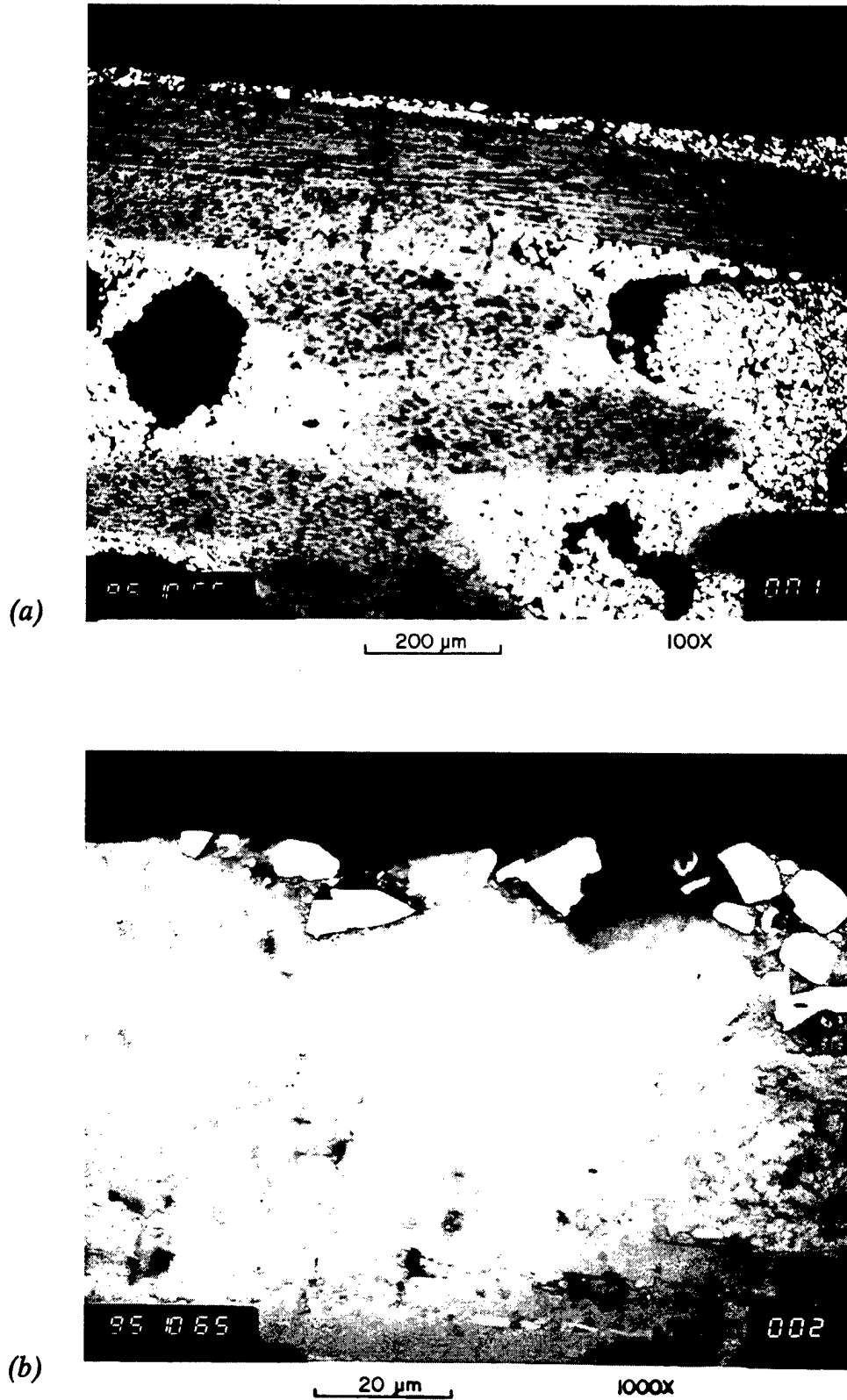
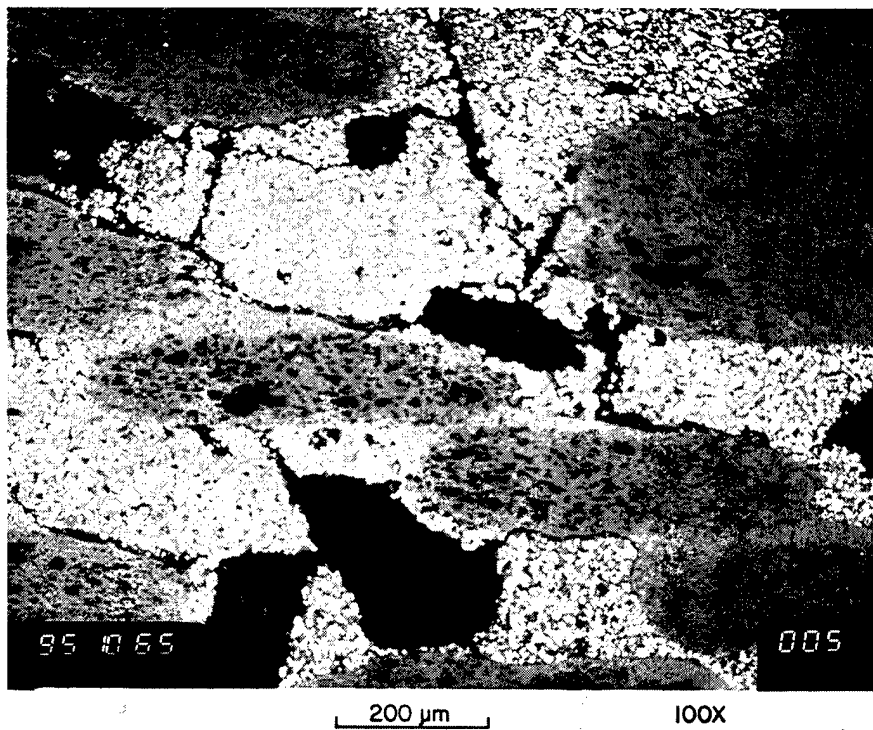


Fig. 19. Photomicrographs at (a) low and (b) high magnification of the outer surface and (c) an area near the center of the wall of the mixed-oxide tube (Babcock & Wilcox designation-tube 7).



**Fig. 19 (continued).** Photomicrographs at (a) low and (b) high magnification of the outer surface and (c) an area near the center of the wall of the mixed-oxide tube (Babcock & Wilcox designation-tube 7).

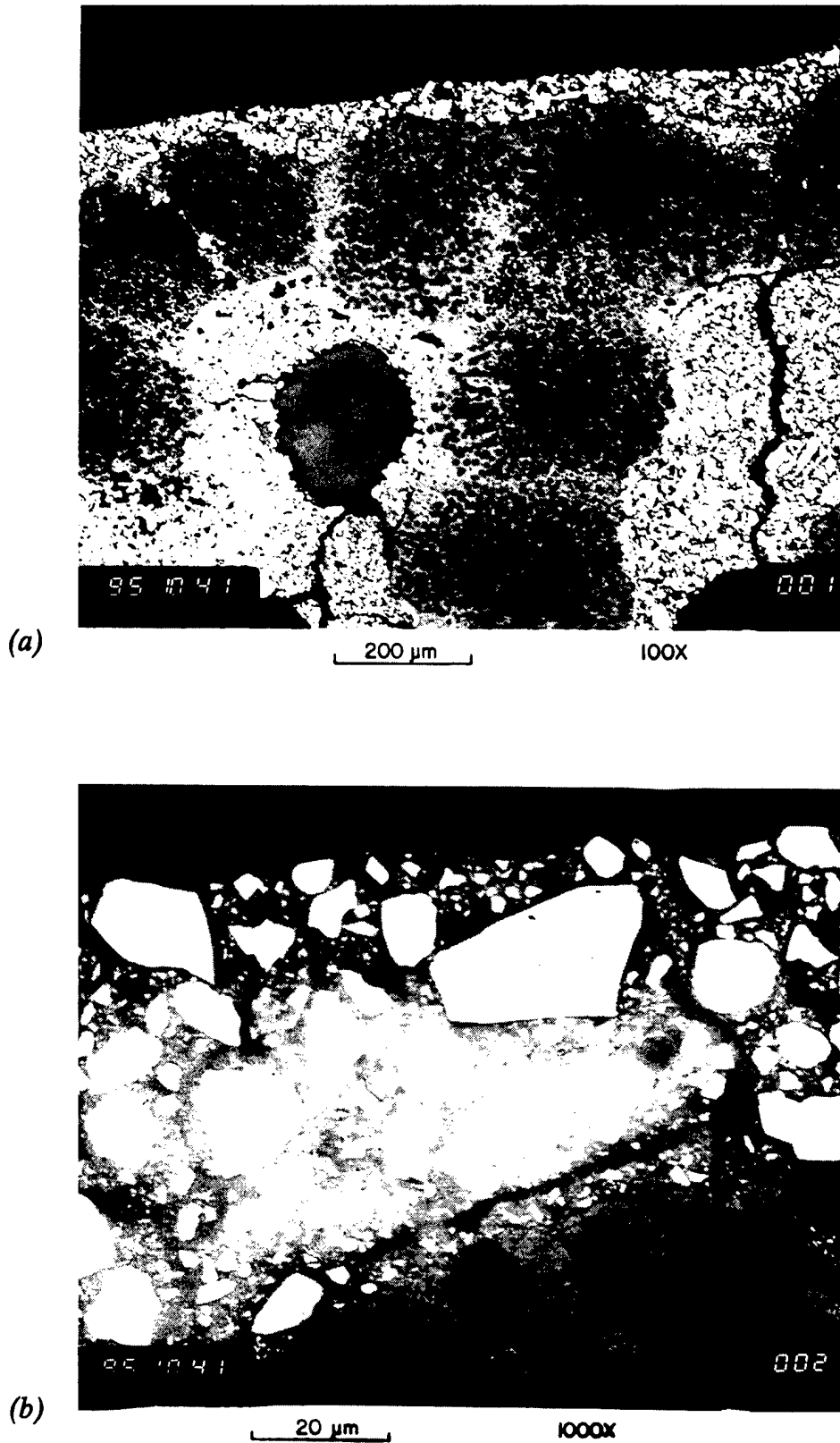
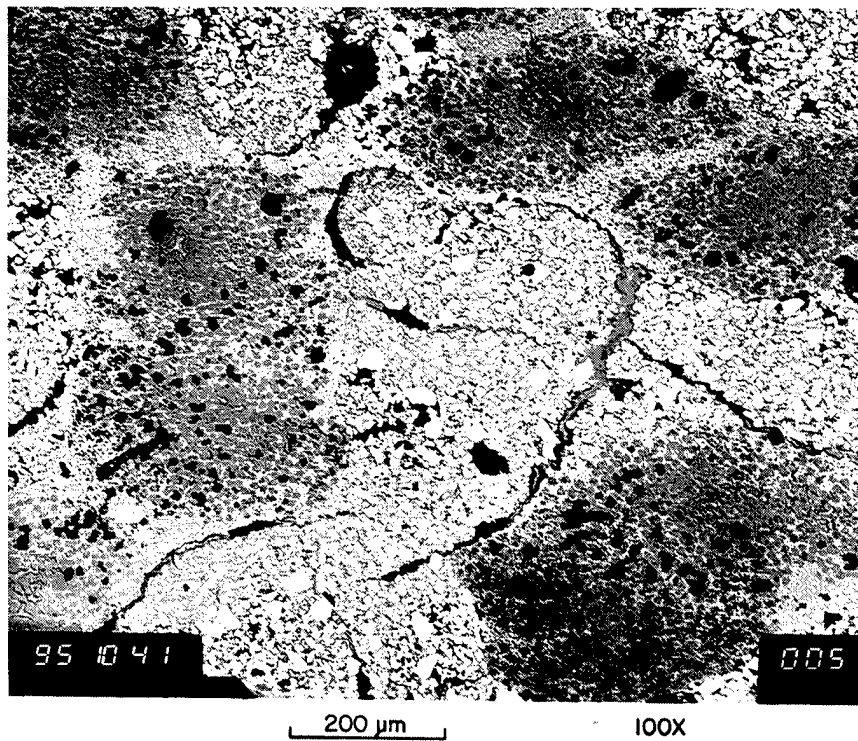


Fig. 20. Photomicrographs at (a) low and (b) high magnification of the tube's outer surface and (c) an area near the center of the wall of the mixed-oxide tube (Babcock & Wilcox designation-tube 9).



**Fig. 20 (continued).** Photomicrographs at (a) low and (b) high magnification of the tube's outer surface and (c) an area near the center of the wall of the mixed-oxide tube (Babcock & Wilcox designation-tube 9).

the incinerator environment. The micrograph taken near the center of the sample shows a significant amount of porosity.

Samples from two tubes of PRD166/zirconia were examined, and micrographs of samples from these tubes are shown in Figs. 16 and 17. The sample from tube 4, shown in the first of these figures, has some porosity near the surface, but there is no evidence of degradation of the fibers that could have resulted from interaction with the environment. The micrograph taken near the center of the sample shows some generally dispersed porosity with evidence of substantial porosity near the interface between two bundles of fibers.

The second PRD166/zirconia tube, tube 5, is shown in the micrographs of Fig. 17, and again there is a small amount of porosity, but in this case the fiber nearest the surface has an indication over half the cross section that it is reacting with the environment. The micrograph of the center of the sample shows porosity along the interface between fiber bundles.

Micrographs of the silicon carbide particulate-strengthened alumina tube are shown in Fig. 18. The surface of this sample has an apparently adherent surface deposit below which is the  $\text{SiC}_p\text{-Al}_2\text{O}_3$  matrix. This subsurface material has essentially no pockets of unreacted aluminum alloy, but farther into the sample, the matrix contains an aluminum-rich alloy [the lightest grey material in Fig. 18(c)] along with the SiC particles. There is some porosity throughout the sample, but the pores are fairly well dispersed and quite small in size.

Samples from each of the two tubes, tubes 7 and 9, composed of the mixed oxide are shown in Figs. 19 and 20, respectively. Figure 19 reveals dark regions in the microstructure of tube 7, containing degraded fibers, with an appreciable amount of porosity and lighter regions that contain angular particles in a matrix. There is also a significant amount of relatively large porosity in the lighter regions. No evidence of interaction of the tube components with the environment is apparent, and the micrograph taken near the center of the sample shows the same structure as the outer surface of the sample with regard to porosity and the light- and dark-colored areas.

Micrographs of the sample from tube 9 are shown in Fig. 20. These micrographs show the same features as seen in Fig. 19 including the porous, dark regions that contain degraded fibers; the light region containing angular particles; and large pores. Again, no evidence of reaction with the environment can be found.

#### 4.4 ELECTRON MICROPROBE EXAMINATION

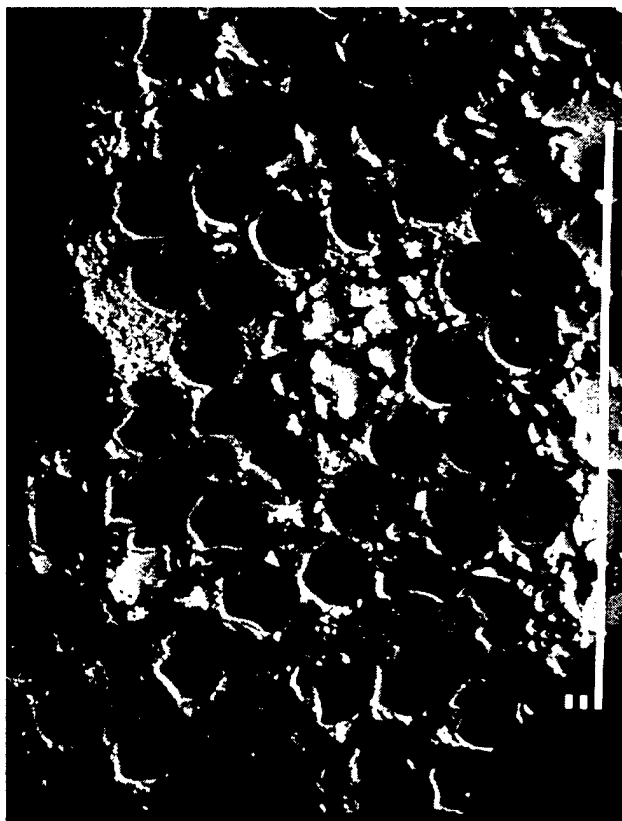
For comparison purposes, samples of the deposits were removed from the surfaces of two of the tubes, PRD166/zirconia tube 5 and silicon carbide particulate- strengthened alumina tube 6, and qualitatively analyzed using energy dispersive X-ray analysis (EDX). These analyses indicated that the surface deposits contained Na, Al, Si, P, S, K, Ca, Ti, and Fe. Concentrations varied somewhat from particle to particle in the powdery material, but all elements were generally present.

In order to identify the elements present on the surface and in the body of each tube, two samples from each tube were examined using an electron microprobe equipped with an EDX system. Figures 21 through 26 provide back-scattered electron (BSE) images and selected elemental dot maps for the samples examined. The BSE images are shown at magnifications of 100 and 800 $\times$ , while all of the dot maps are taken at 800 $\times$ , and cover the same area as shown in the higher magnification BSE images.

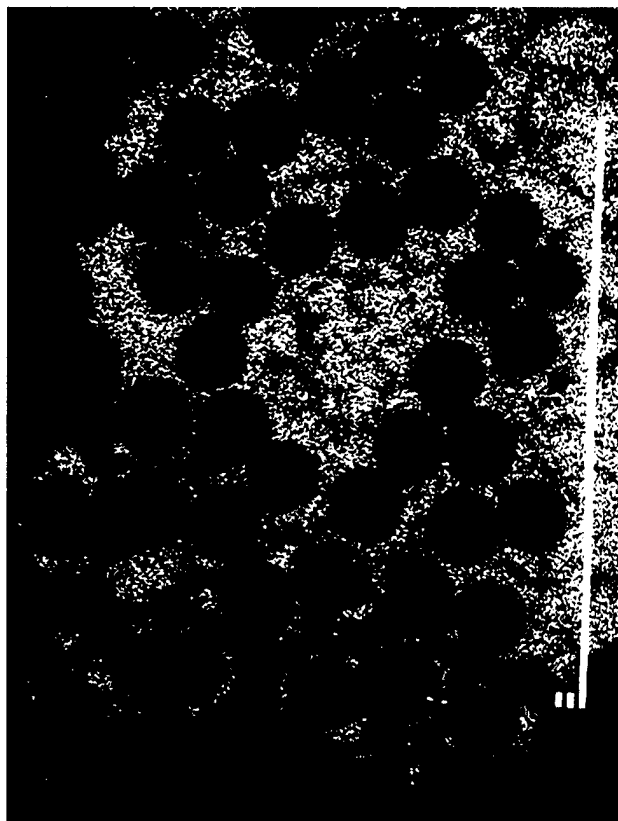
Examination of the samples of Nextel 610/zirconia showed the composite was composed of a zirconia matrix surrounding alumina fibers as presented in Fig. 21. Neither the transverse nor longitudinal sections showed any significant evidence of interaction between the gases in the incinerator environment and the composite materials. Deformation of the alumina fibers near the edge of the mounted samples was apparently due to chipping of the loosely supported fibers during grinding and polishing. An aluminum map does not indicate a loss of aluminum from the deformed fibers. A slightly elevated concentration of the scale constituents was found along the edge of the specimens, but only silicon appeared to intrude into the matrix of the sample. This silicon is most likely a contaminant resulting from the polishing operation.

The Almax/zirconia composite was composed of a zirconia matrix with alumina fibers as shown in Fig. 22. No significant interaction between the incinerator gases and the composite materials was observed. Near the center of one of the samples, elevated levels of K, Ca, Na, and S were detected. However, more extensive examination led to the conclusion that these elements were present as a result of contamination rather than diffusion or interaction.

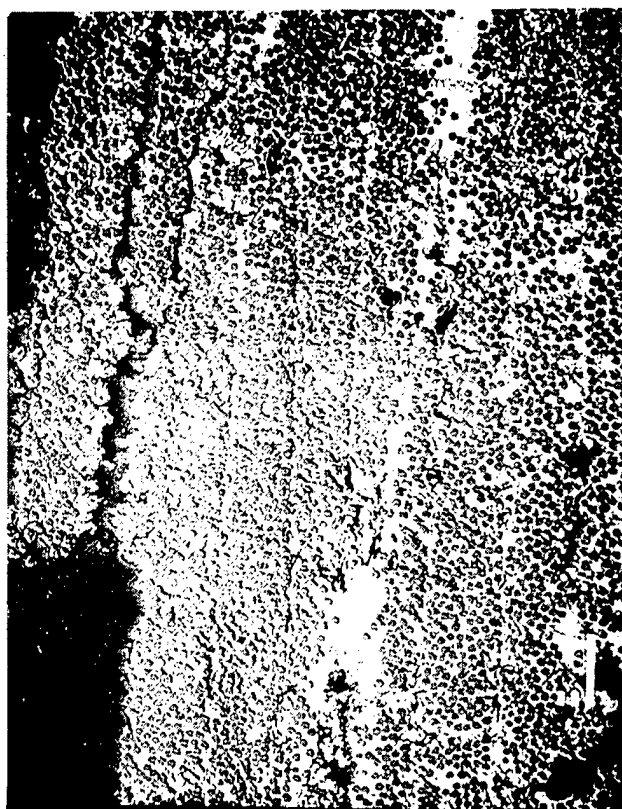
Samples from two PRD166/zirconia tubes were examined, and there were significant differences in the observations. Analysis of one of the samples (see Fig. 23) indicated the composite was composed of a zirconia matrix with fibers of alumina containing a low concentration of zirconia. No evidence of significant interaction was observed between the composite material and the incinerator gases. However, some intrusion of K and P was detected near the surface.



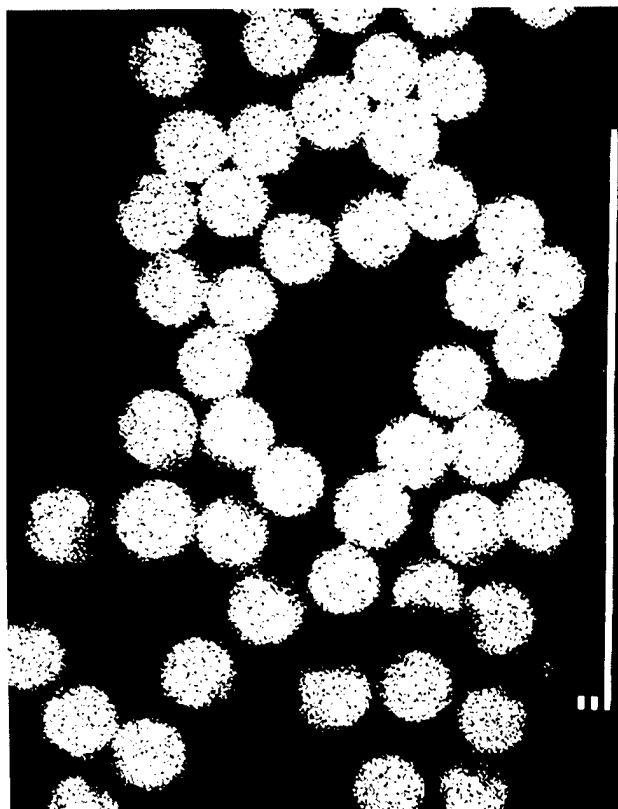
Back-scattered electron image



Zr elemental dot map

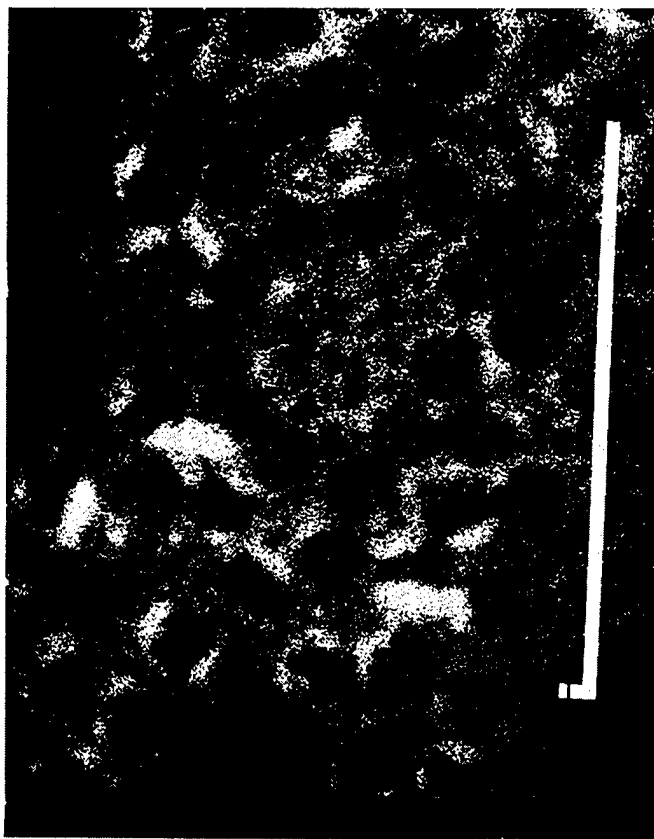


Back-scattered electron image



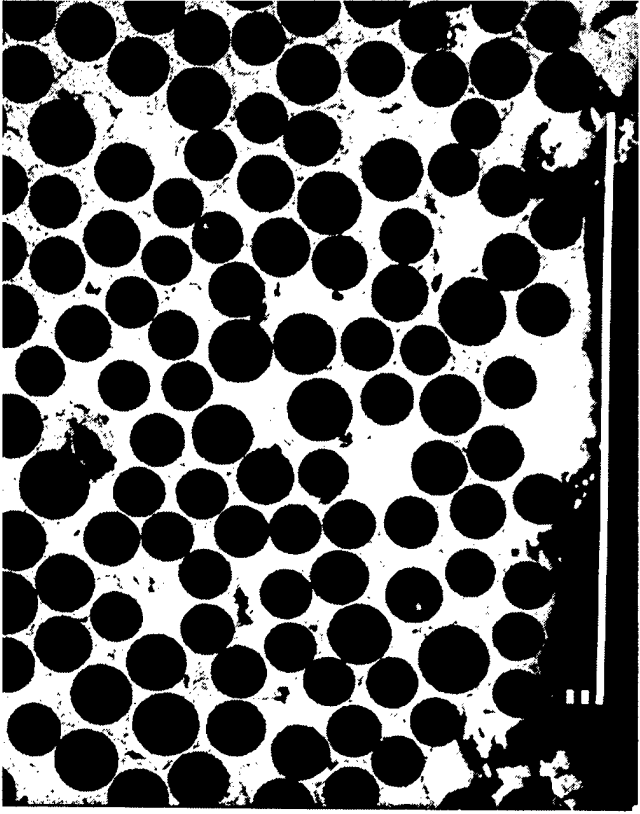
Al elemental dot map

Fig. 21. Back-scattered electron image and Al, Zr, and Si elemental dot maps for Nextel 610/zirconia sample.

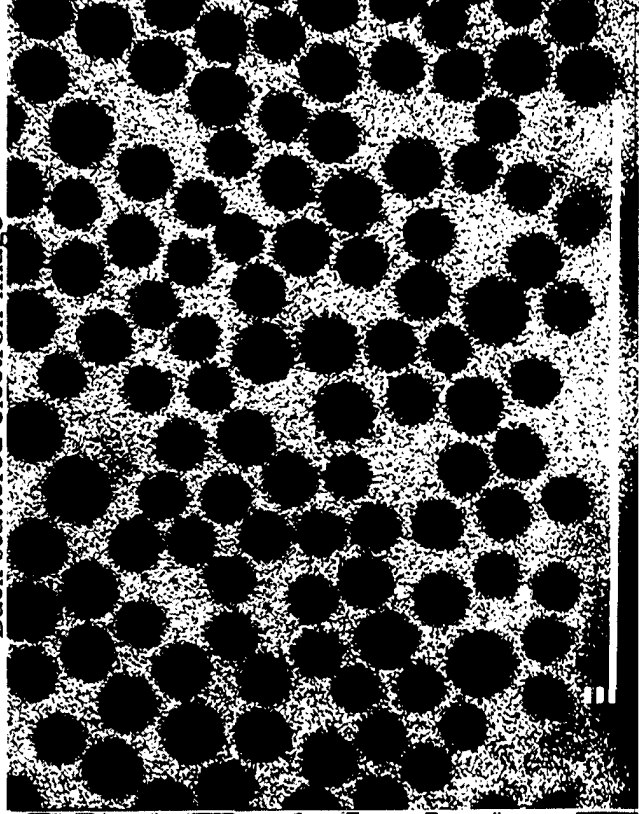


Si elemental dot map

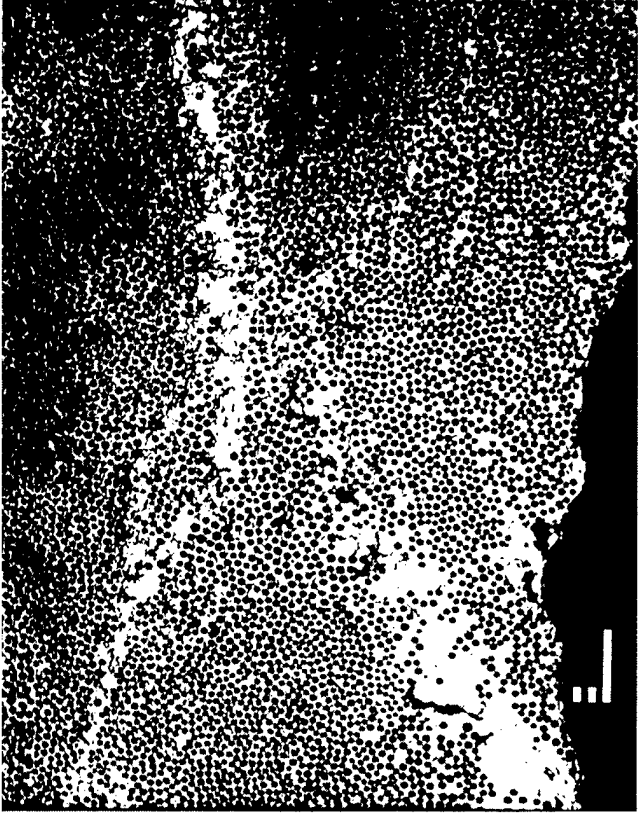
Figure 21 (continued) Back-scattered electron image and Al, Zr and Si elemental dot maps for Nextel 610/zirconia sample.



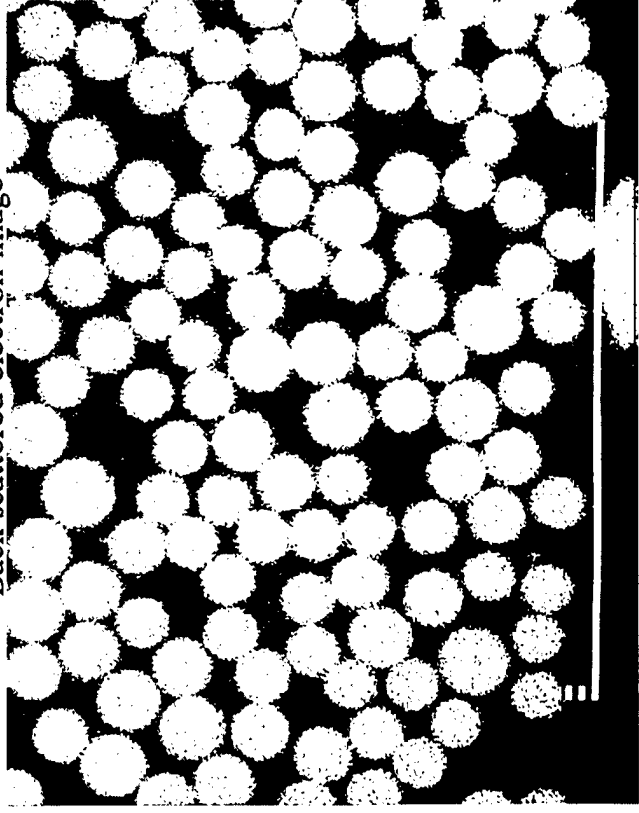
Back-scattered electron image



Zr elemental dot map



Back-scattered electron image



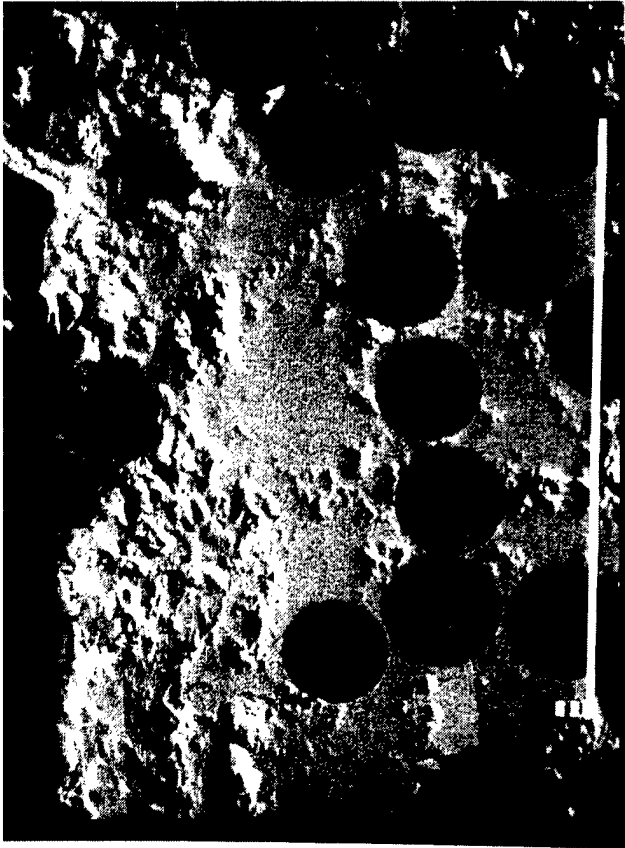
Al elemental dot map

Figure 22 Back-scattered electron image and Al, Zr and Si elemental dot maps for Almax/zirconia sample.

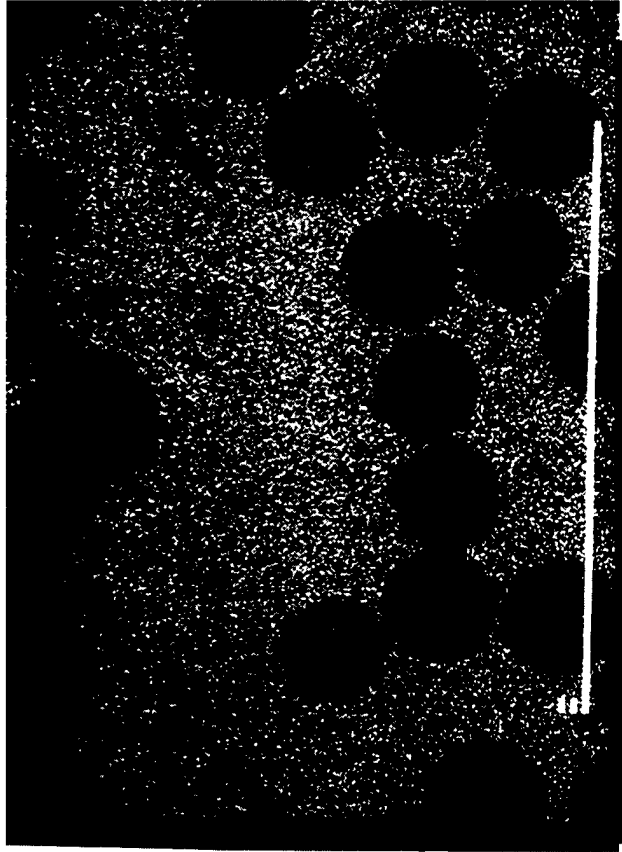


Si elemental dot map

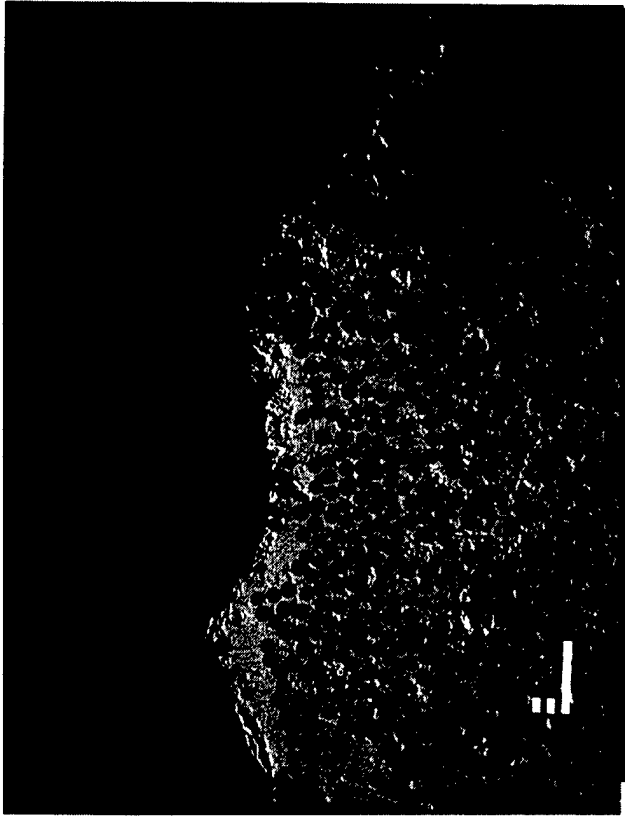
Figure 22 (continued) Back-scattered electron image and Al, Zr and Si elemental dot maps for Almax/zirconia sample.



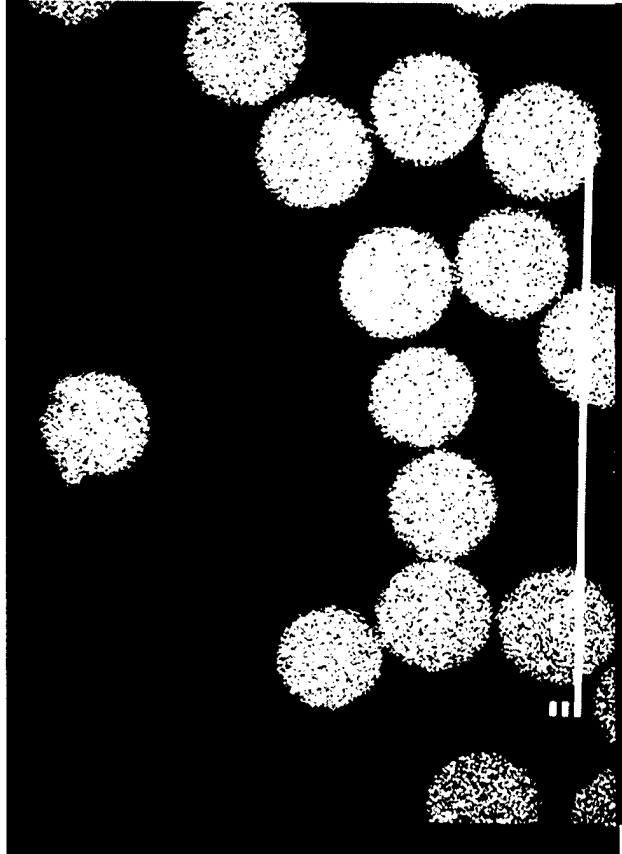
Back-scattered electron image



Zr elemental dot map

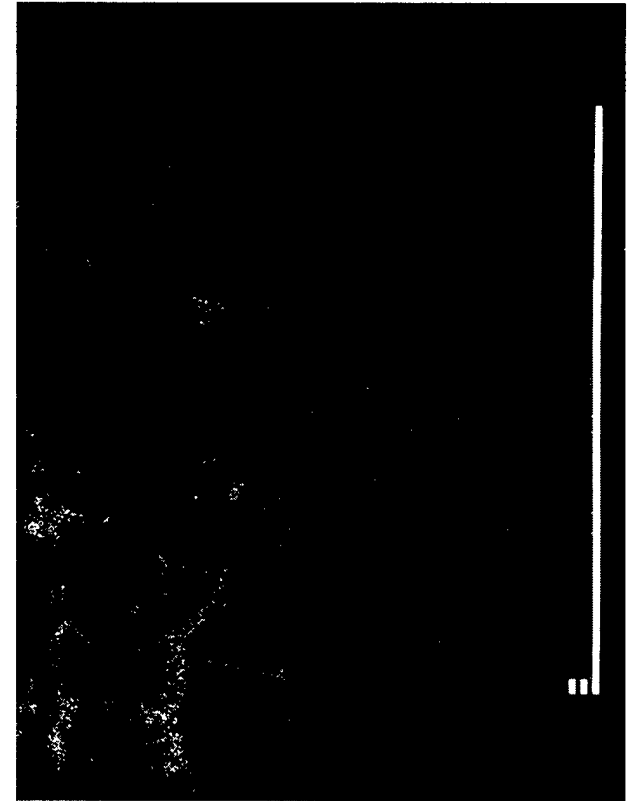


Back-scattered electron image

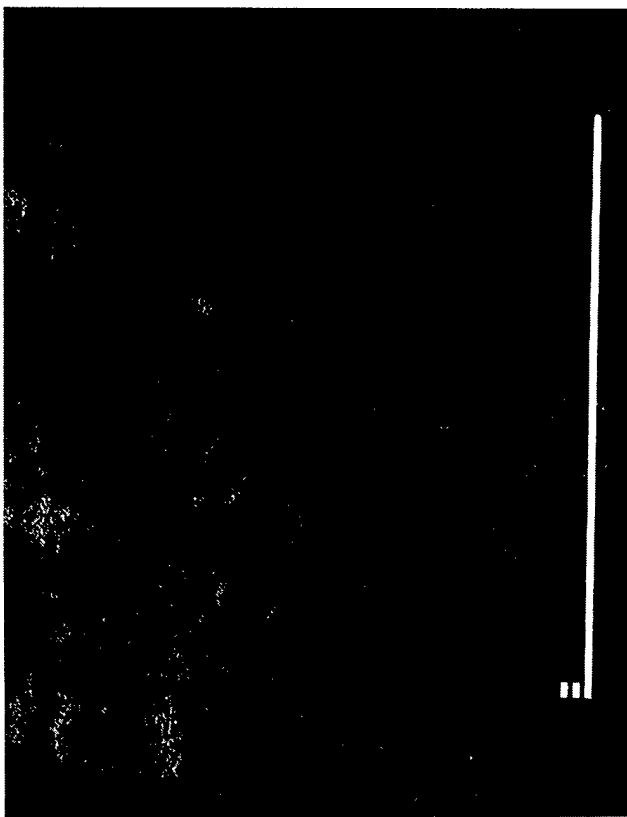


Al elemental dot map

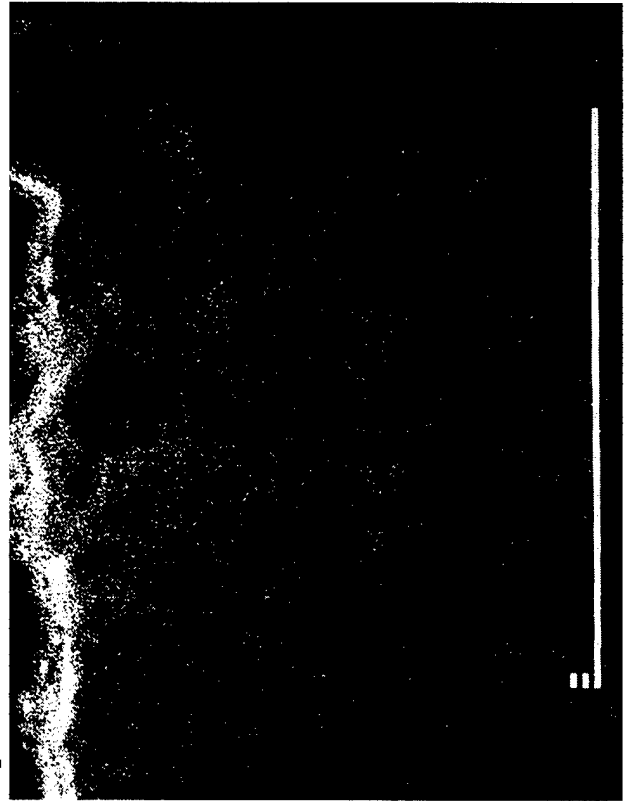
Figure 23 Back-scattered electron image and Al, Zr, Si, K, and P elemental dot maps for PRD166/zirconia tube 4.



K elemental dot map



Si elemental dot map

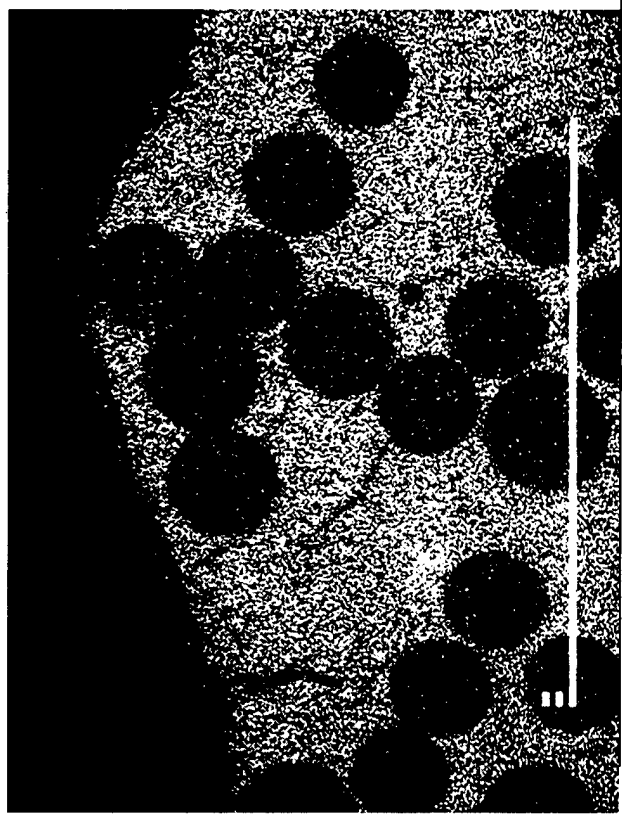


P elemental dot map

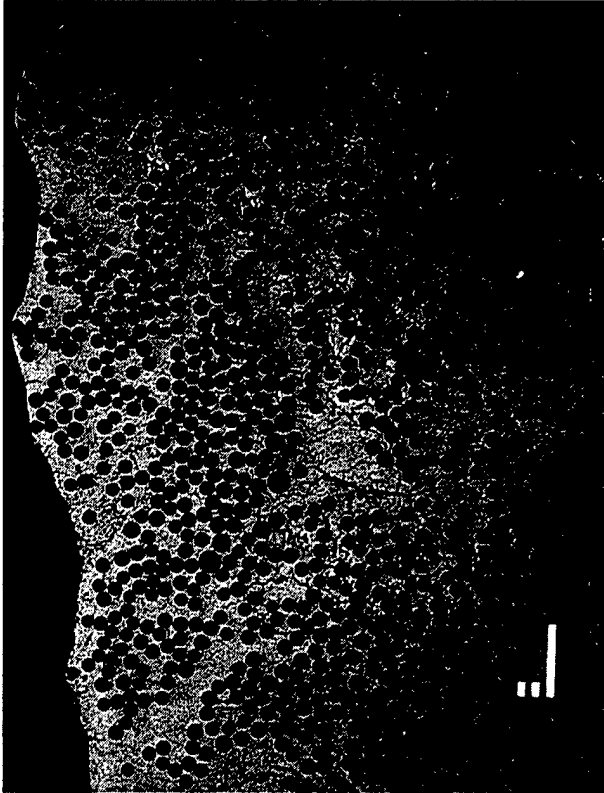
Figure 23 (continued) Back-scattered electron image and Al, Zr, Si, K, and P dot maps for PRD166/zirconia tube 4.



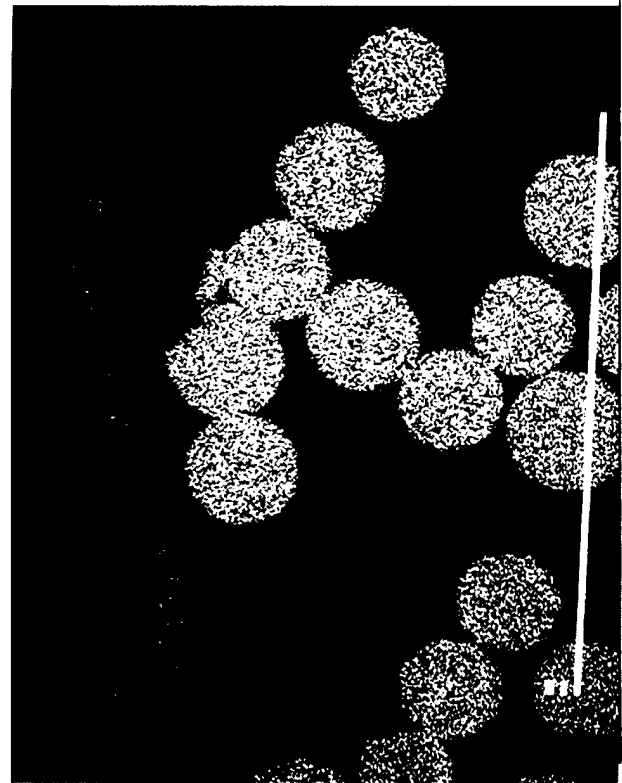
Back-scattered electron image



Zr elemental dot map

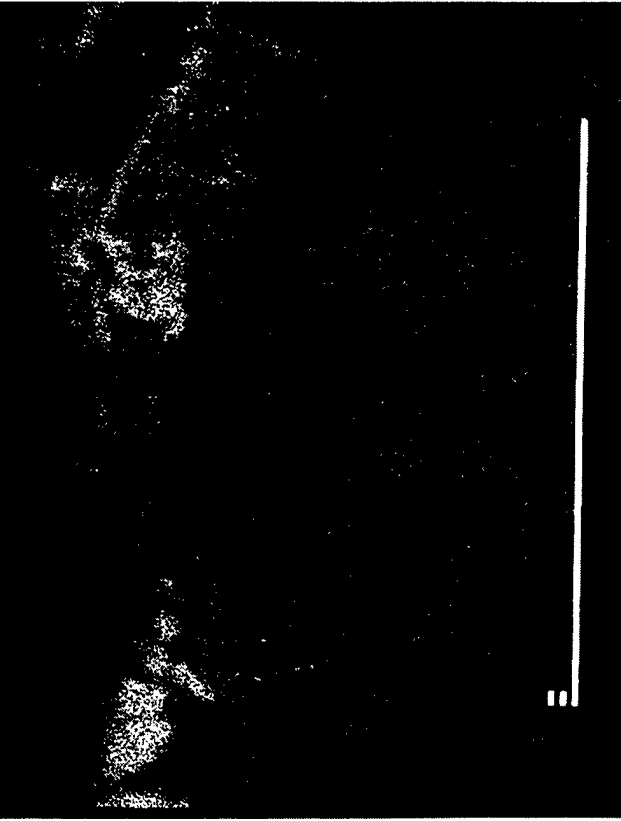


Back-scattered electron image

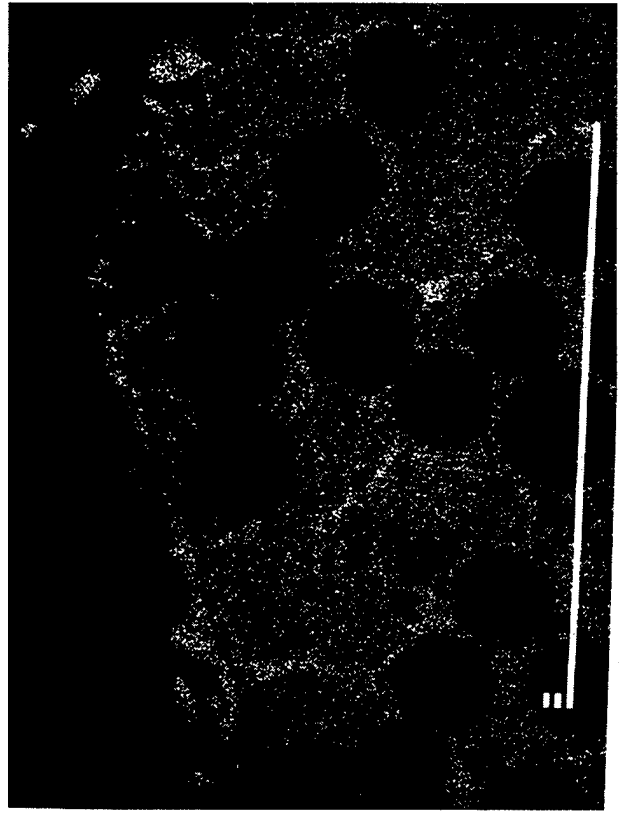


Al elemental dot map

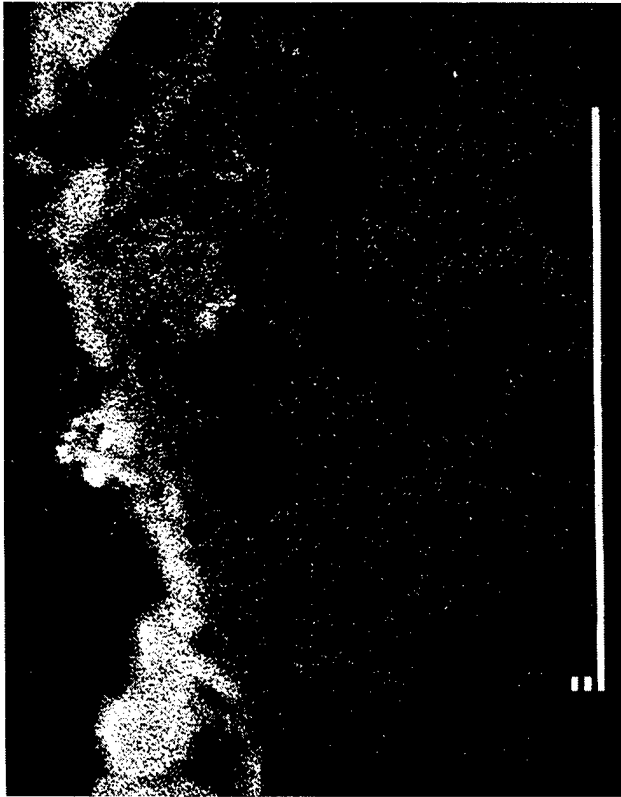
Figure 24 Back-scattered electron image and Al, Zr, Si, K, and P dot maps for PRD166/zirconia sample (tube 5).



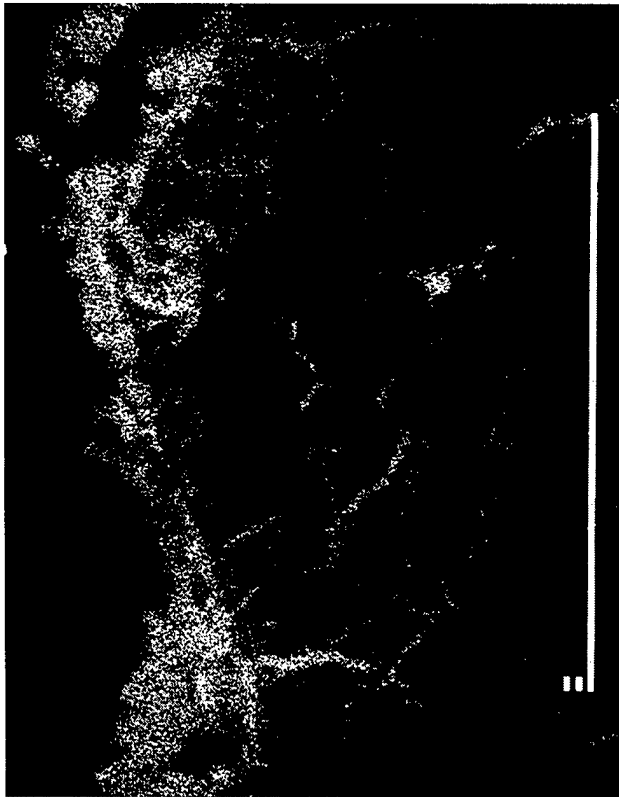
K elemental dot map



Y elemental dot map

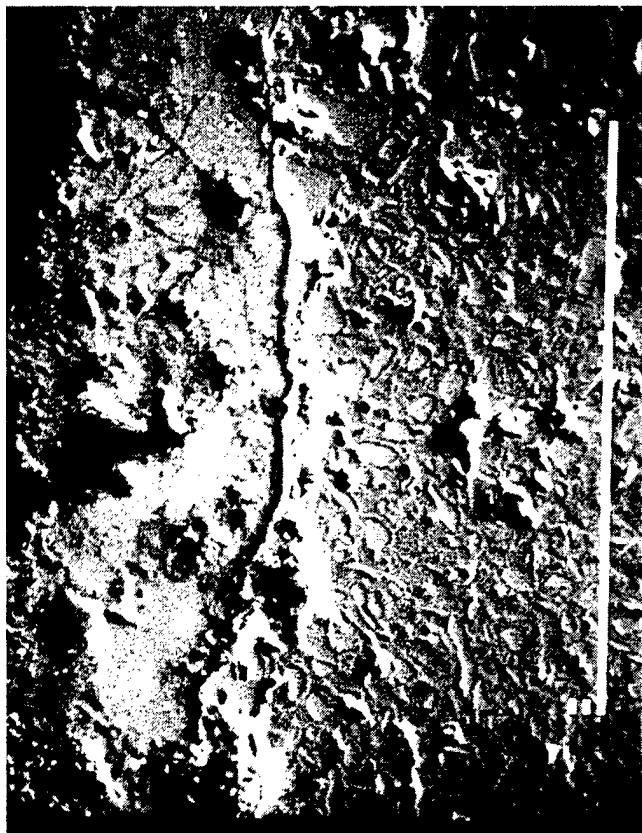


Si elemental dot map

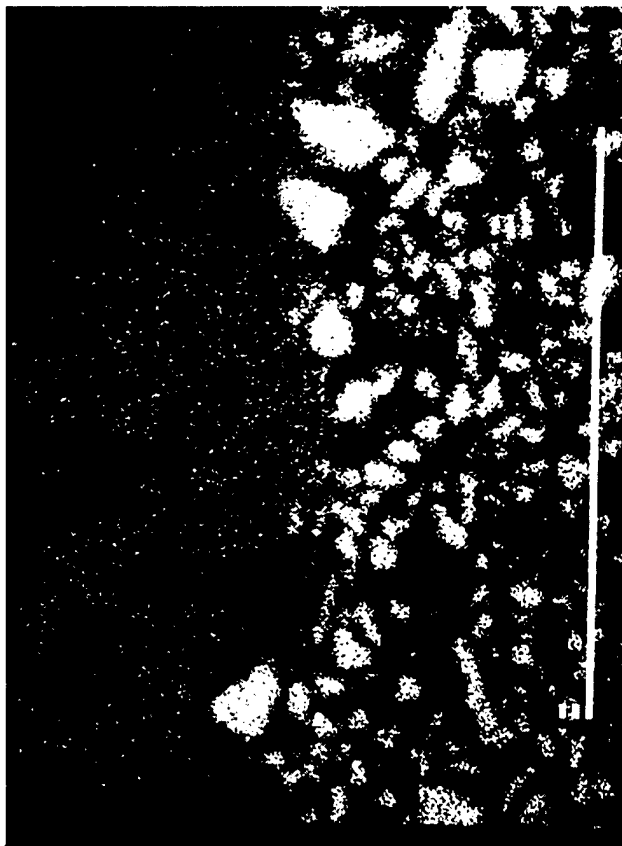


P elemental dot map

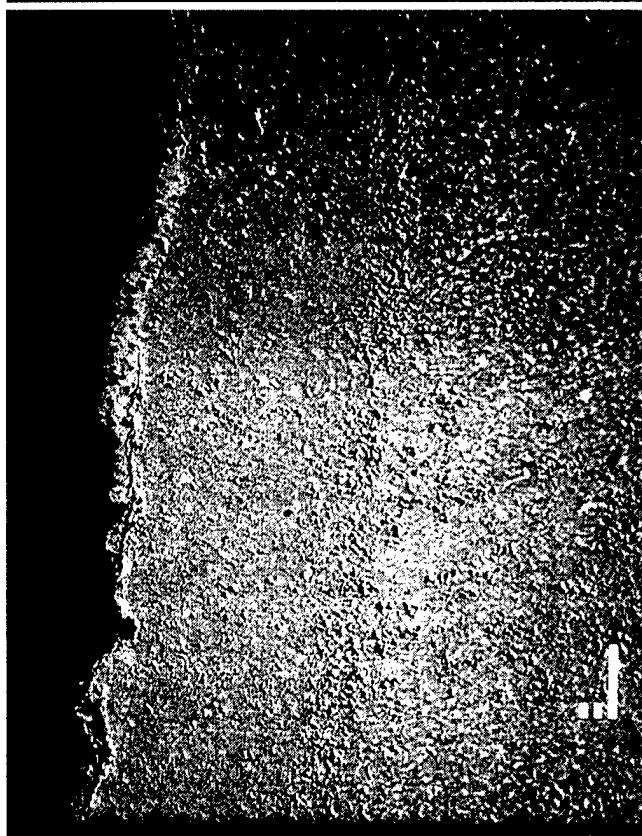
Figure 24 (con't) Back-scattered electron image and Al, Zr, Si, K, P and Y dot maps for PRD166/zirconia sample (tube 5).



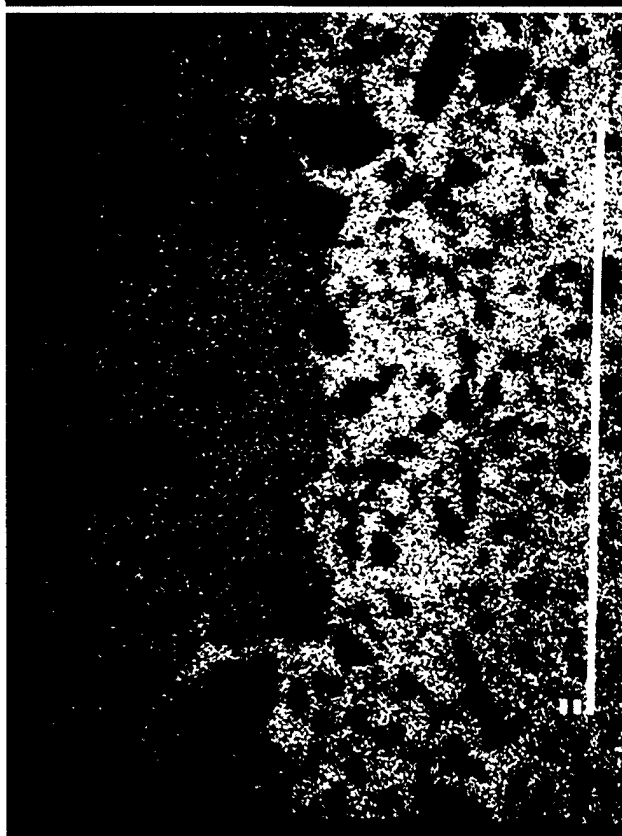
Back-scattered electron image



Si elemental dot map

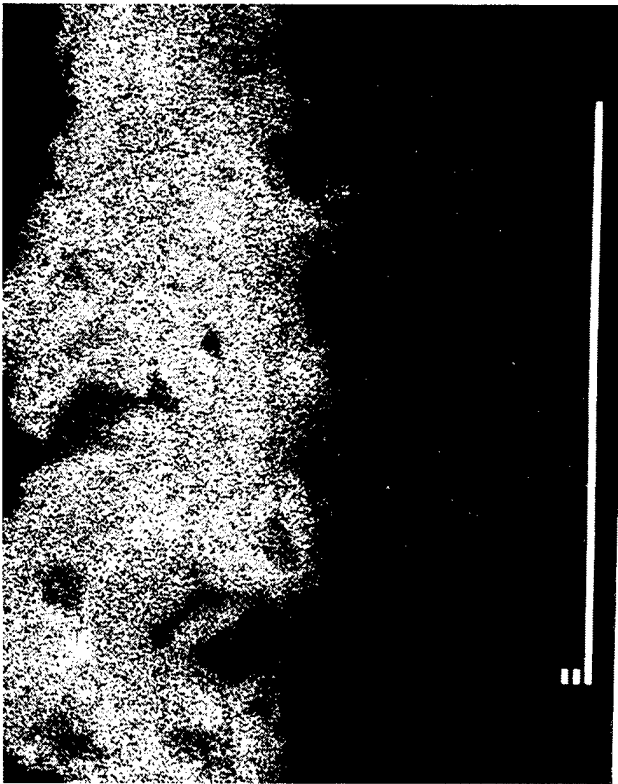


Back-scattered electron image

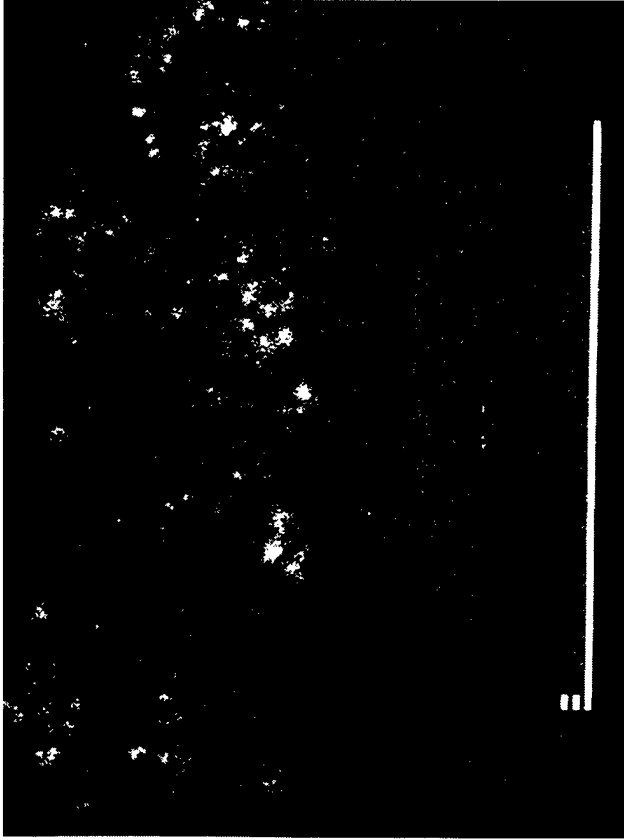


Al elemental dot map

Figure 25 Back-scattered electron image and Al, Zr, Si, K, and P dot maps for the SiC<sub>p</sub>-Al<sub>2</sub>O<sub>3</sub> sample.



P elemental dot map



Ti elemental dot map

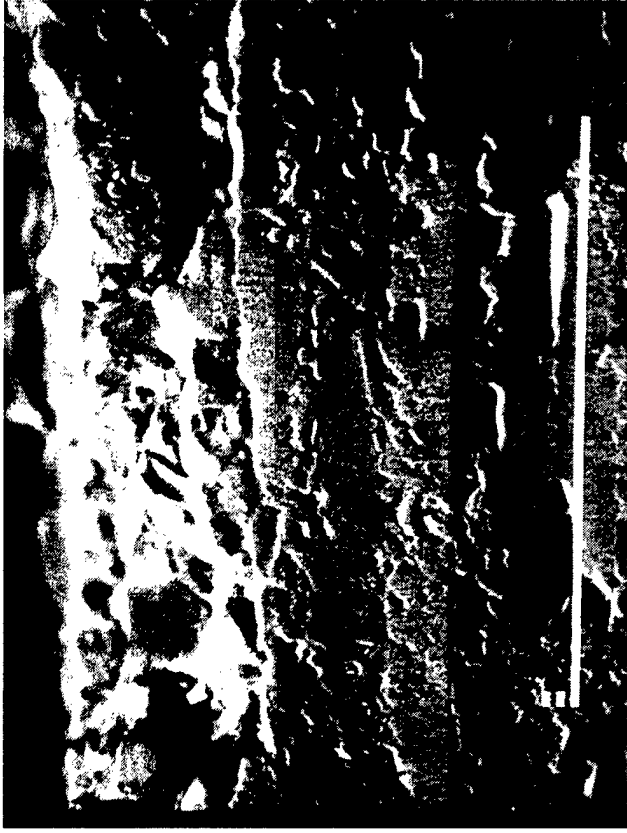


K elemental dot map



C elemental dot map

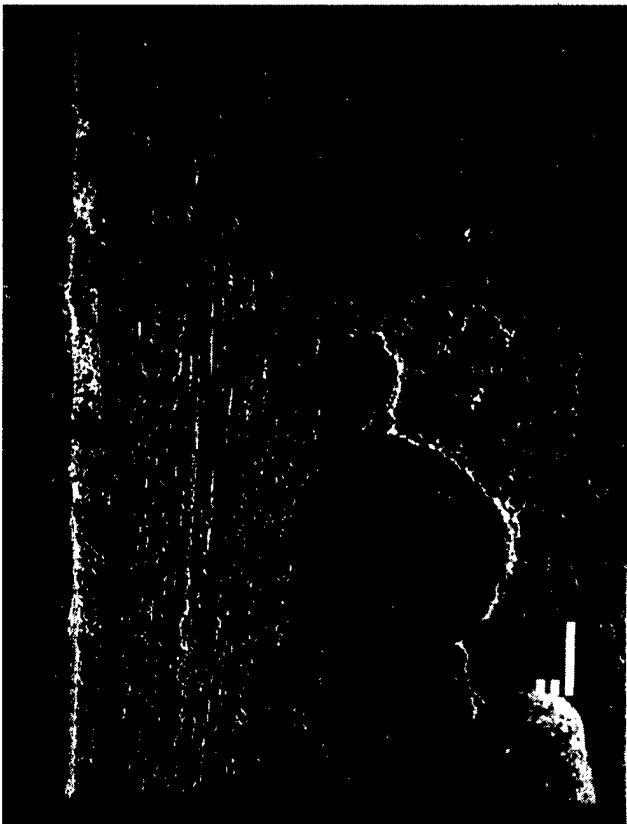
Figure 25 (con't) Back-scattered electron image and Al, Si, K, P, Ti and C dot maps for the SiC<sub>F</sub>-Al<sub>2</sub>O<sub>3</sub> sample.



Back-scattered electron image



Si elemental dot map

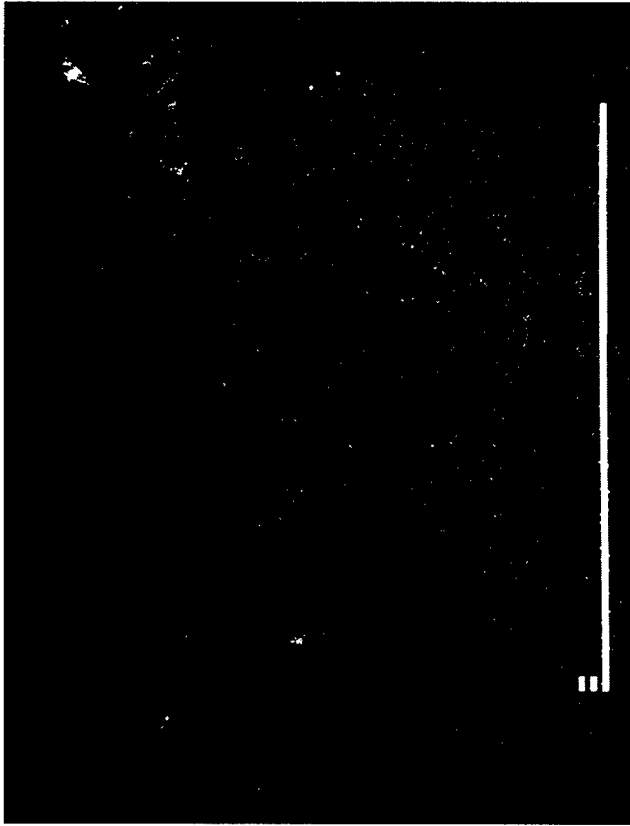


Back-scattered electron image

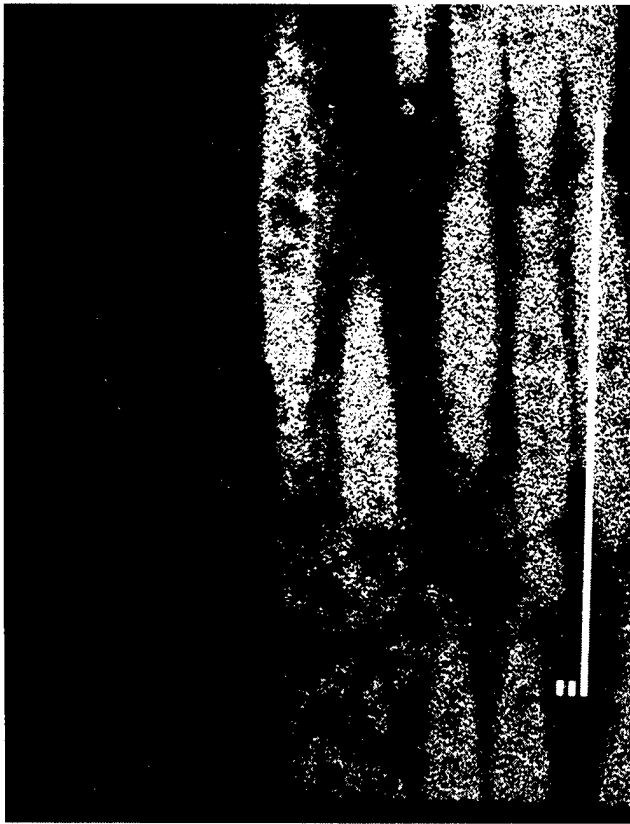


Al elemental dot map

Figure 26 Back-scattered electron image and Al, Si, Mg, K, and C dot maps for the mixed oxide sample.



K elemental dot map



Mg elemental dot map



C elemental dot map

Figure 26 (continued) Back-scattered electron image and Al, Si, K, P, Ti and C dot maps for the mixed oxide sample.

The second PRD166/zirconia tube had the same composition of the phases as the sample just described (see Fig. 24); however, two types of reaction between the incinerator gases and the composite material were indicated. Fibers that had their surfaces exposed showed areas of aluminum depletion and deposits of K, P, Si, Ca and S in the alumina-depleted location. Segregation of Y from the matrix to form a thin Y-P- rich layer along the surface was observed. The Y-P was also observed to segregate along thin lines that penetrated well into the zirconia matrix.

The particulate-strengthened composite, as shown in Fig. 25, was determined to consist of an alumina matrix containing particles of silicon carbide that ranged in size from 5 to approximately 20  $\mu\text{m}$ . A layer up to 50  $\mu\text{m}$  in thickness containing relatively uniform concentrations of Al, Si, K, Na, P, S, and Ca, along with particles rich in Ti, covered the outer surface of the specimen. Some K was detected below the sample's surface, but this was likely associated with contamination transferred during polishing. No evidence of interaction of the incinerator gases with the composite components was detected.

The composite identified as Type B mixed oxide consisted of the remnants of fibers of Si, Mg, and Al in an alumina matrix along with regions, including the outer surface, as shown in Fig. 26, that contained Si and C. No significant interaction was observed, but an increased concentration of Na and P was detected between the outer surface layer and the composite. Some small spots rich in K were observed in the matrix.

Following the initial review of results, several other issues were addressed by means of additional microprobe examinations of these exposed samples and the unexposed sample of PRD166/zirconia tubing that was subsequently provided by B & W.

The porosity in the Nextel 610/zirconia and in the Almax/zirconia was examined, and it was concluded that the Nextel-containing sample contained large, irregular voids throughout while the Almax-containing sample had voids that appeared as cracks along relatively wide bands of the matrix material. These crack-like voids did not appear to contain as much volume as the larger voids in the Nextel/zirconia sample. Both specimens contained fine porosity, and no significant difference in this regard was determined.

A question was also raised about the difference in porosity of the fibers for both the Nextel and the Almax fibers. BSE and secondary electron images taken of both fibers at 2000 $\times$  did not reveal any porosity in either of the samples.

The electron microprobe was also used to further study the distribution of Y in the samples, and particularly in the PRD166/zirconia samples. A recheck of the first PRD166/zirconia tube showed that Y was present in the zirconia matrix of that sample, but it was not segregated in the manner observed in the second of the PRD166/zirconia samples. Examination of the unexposed sample of PRD166/zirconia showed that Y was present in the matrix of the sample, but it was not segregated to surfaces, cracks, or any other microstructural feature. A check of the other ceramic fiber/ceramic composite samples examined in this study showed no Y was present in the Nextel 610/zirconia sample, but Y was present in the Almax/zirconia sample.

## 5. DISCUSSION AND CONCLUSIONS

Without complete data from c-ring tests on unexposed samples of all these materials, it is impossible to say if exposure to the incinerator environment affected the strength of the composites. Tests of the unexposed PRD166/zirconia sample resulted in a lower strength than measured on the exposed samples, so it appears that exposure did not degrade the strength of the PRD166/zirconia composite. Likewise, for the silicon carbide particulate-strengthened alumina, unpublished results from other incinerator corrosion studies<sup>6</sup> indicate that the strength of this composite was not significantly degraded by the incinerator exposure.

Except for the PRD166/zirconia samples, no evidence was found of any reaction of the composite materials with the components of the incinerator effluent. This absence of evidence of reaction of the tube materials with the environment provides short-time data that are consistent with no degradation of the mechanical strength of the composites. For the PRD166/zirconia samples, some interaction with the environment was observed, but, as in previous studies, it only occurred in fibers that were in close proximity to the surface. Although some degradation of these fibers seems to be occurring, the extent of degradation is so limited that it is unlikely that it will have a significant impact on the performance of the composite.

## 6. REFERENCES

1. J. K. Keiser, J. I. Federer, T. J. Henson, and D. L. Hindman, *High Temperature Corrosion of Ceramic-Ceramic Composites in a Waste Incinerator Environment*, ORNL/TM-12212, Martin Marietta Energy Systems, Inc., Oak Ridge Natl. Lab., January 1993.
2. D. L. Hindman, H. L. Wishkoff, and D. J. Landini, "Corrosion of Ceramic Composite Heat Exchanger Materials in a Hazardous Waste Incinerator," *CORROSION/93*, Paper No. 199, National Association of Corrosion Engineers, Houston, March 1993.
3. D. L. Hindman and J. R. Keiser, "Performance of Ceramic-Ceramic Composites in an Industrial Waste Incinerator," *CORROSION/94*, Paper No. 191, National Association of Corrosion Engineers, Houston, March 1994.
4. D. J. Landini, DuPont Lanxide Composites, Newark, Del., personal communication to J. R. Keiser, Lockheed Martin Energy Systems, Oak Ridge Natl. Lab., Oak Ridge, Tenn.
5. M. K. Ferber, V. J. Tennery, S. B. Waters, and J. Ogle, "Fracture Strength Characterization of Tubular Ceramic Materials Using a Simple C-ring Geometry," *J. Mat. Sci.*, **21**, 2628-32 (1986).
6. J. R. Keiser, unpublished data, 1994-95.

## 7. ACKNOWLEDGMENTS

The authors thank S. J. Pawel, D. F. Wilson, and J. R. DiStefano for technical review; K. Spence for technical editing; and M. R. Upton for final manuscript preparation.

## INTERNAL DISTRIBUTION

- |                                    |                                  |
|------------------------------------|----------------------------------|
| 1-2. Central Research Library      | 23-29. J. R. Keiser              |
| 3. Document Reference Section      | 30. E. Lara-Curzio               |
| 4-5. Laboratory Records Department | 31. H. F. Longmire               |
| 6. Laboratory Records, ORNL RC     | 32. R. A. Lowden                 |
| 7. ORNL Patent Section             | 33. J. R. Mayotte                |
| 8-10. M&C Records Office           | 34. A. E. Pasto                  |
| 11. R. L. Beatty                   | 35. S. J. Pawel                  |
| 12. P. F. Becher                   | 36. W. D. Porter                 |
| 13. T. M. Besmann                  | 37. P. S. Sklad                  |
| 14. R. A. Bradley                  | 38. D. P. Stinton                |
| 15. N. C. Cole                     | 39. P. F. Tortorelli             |
| 16. D F. Craig                     | 40. L. R. Walker                 |
| 17. J. H. DeVan                    | 41. A. Wereszczak                |
| 18. J. R. DiStefano                | 42. D. F. Wilson                 |
| 19. M. K. Ferber                   | 43. H. W. Folgesong (Consultant) |
| 20. F. M. Foust                    | 44. E. L. Menger Consultant)     |
| 21. M. L. Grossbeck                | 45. K. E. Spear (Consultant)     |
| 22. M. A. Karnitz                  |                                  |

## EXTERNAL DISTRIBUTION

46. AMERCOM/ATLANTIC RESEARCH CORPORATION, 8928 Fullbright Avenue, Chatsworth, GA 91311-6180  
W. E. Beyermann
47. ARGONNE NATIONAL LABORATORY, 9700 S. Cass Avenue, Argonne, IL 60439-4815  
W. A. Ellingson
- 48-49. BABCOCK & WILCOX, R&D Division, 1562 Beeson Street, Alliance, OH 44601  
C. L. DeBellis  
J. B. Sandifer
- 50-57. BABCOCK & WILCOX, P.O. Box 11165, Lynchburg, VA 24505  
D. L. Baty  
R. W. Goettler  
D. L. Hindman (5)  
W. G. Long

58-59. CARBORUNDUM COMPANY, P.O. Box 1054, Niagara Falls, NY 14302

J. M. Bevilacqua  
M. C. Kerr

60. CONSOLIDATED NATURAL GAS, 11001 Cedar Avenue, Cleveland,  
OH 44106

J. Bjerklie

61. DOW CORNING CORPORATION, 3901 South Saginaw Road, Midland,  
MI 48640

W. H. Atwell

62. DREXEL UNIVERSITY, Building 27-439, Philadelphia, PA 19104

63-65. DuPONT LANXIDE COMPOSITES, 1300 Marrows Road, P.O. Box 6077,  
Newark, DE 19714-6077

D. J. Landini  
A. N. Patel (MS-6077)  
J. K. Weddell

66-67. GAS RESEARCH INSTITUTE, 8600 W. Bryn Mawr Avenue, Chicago,  
IL 60631

S. Freedman  
M. A. Lukasiewicz

68. GENERAL ELECTRIC COMPANY, GE Corporate Research and  
Development, P.O. Box 8, Schenectady, NY 12301

F. N. Mazandarany, Bldg. K-1, MB-259

69. MASSACHUSETTS INSTITUTE OF TECHNOLOGY, 77 Massachusetts  
Avenue, Room 12-009, Cambridge, MA 02139

J. S. Haggerty

70-71. NORTON COMPANY, 1 New Bond Street, Worcester, MA 01606

B. D. Foster  
K. Green

72. PAR ENTERPRISE, INCORPORATED, 12601 Clifton Hunt Lane, Clifton,  
VA 22024

W. J. Rebello

73. PENNSYLVANIA STATE UNIVERSITY, 227 Hammond Building,  
University Park, PA 16802  
H. T. Hahn
74. PENNSYLVANIA STATE UNIVERSITY, 513A Deike Building,  
University Park, PA 16802  
J. R. Hellmann
- 75-76. REFRACTORY COMPOSITES, INCORPORATED, 12220-A Rivera Road,  
Whittier, CA 90606  
K. Kratsch  
E. L. Paquette
- 77-79. SOLAR TURBINES, INCORPORATED, P.O. Box 85376, San Diego,  
CA 92138-5376
- 80-81. STONE & WEBSTER ENGINEERING CORPORATION, 1430 Enclave  
Parkway, Houston, TX 77077-2023  
D. T. Arnold  
J. M. Gondolfe
82. TEXTRON SPECIALTY MATERIALS, 2 Industrial Avenue, Lowell,  
MA 01851  
B. Thomson
83. UNIVERSITY OF ILLINOIS AT CHICAGO, P.O. Box 4348, Chicago,  
IL 60680  
M. J. McNallan
84. UNIVERSITY OF TENNESSEE SPACE INSTITUTE (UTSI), MS 3,  
Tullahoma, TN 37388  
W. H. Boss
- 85-86. U.S. DOE, CHICAGO FIELD OFFICE, 9800 S. Cass Avenue, Argonne,  
IL 60439  
J. E. Jonkouski  
J. Mavec
- 87-88. U.S. DOE, MORGANTOWN ENERGY TECHNOLOGY CENTER, P.O.  
Box 880, Morgantown, WV 26505  
C. T. Alsup, Jr.  
R. A. Bajura

- 89-92. U.S. DOE, OFFICE OF INDUSTRIAL TECHNOLOGIES,  
1000 Independence Avenue, Forrestal Building, Washington, DC 20585
- G. M. Varga, Jr.  
W. P. Parks, Jr.  
S. L. Richlen  
M. A. Smith
93. U.S. DOE, OFFICE OF BASIC ENERGY SCIENCES, Materials Sciences  
Division, ER-131 GTN, Washington, DC 20545
- J. B. Darby
94. U.S. DOE, OFFICE OF FOSSIL ENERGY, Technical Coordinator, FE-14,  
B114 GTN, Washington, DC 20585
- J. P. Carr, (FE-14) GTN
95. U.S. DOE, OFFICE OF ENERGY EFFICIENCY AND RENEWABLE  
ENERGY, CE-12 Forrestal Building, Washington, DC 20545
- J. J. Eberhardt
- 96-99. U.S. DOE, PITTSBURGH ENERGY TECHNOLOGY CENTER, P.O.  
Box 10940, Pittsburgh, PA 15236
- A. H. Baldwin  
G. V. McGurl  
R. Santore  
T. M. Torkos
100. U.S. DOE, OAK RIDGE OPERATIONS OFFICE, P.O. Box 2008,  
Building 4500N, MS 6269, Oak Ridge, TN 37831
- M. H. Rawlins
- 101-110. U.S. DOE, OFFICE OF SCIENTIFIC AND TECHNICAL INFORMATION,  
P.O. Box 62, Oak Ridge, TN 37831
111. OFFICE OF ASSISTANT MANAGER, ENERGY RESEARCH AND  
DEVELOPMENT, P.O. Box 2008, Oak Ridge, TN 37831-8600
- For distribution by microfiche as shown in DOE/OSTI-4500,  
Distribution Category UC-310 Industrial Programs (General)

M98054270



Report Number (14) ORNL/TM--13128

\_\_\_\_\_  
\_\_\_\_\_  
\_\_\_\_\_

Publ. Date (11) 199606

Sponsor Code (18) DOE/EE, XF

UC Category (19) UC-1400, DOE/ER

*ph*

DTIC QUALITY INSPECTED 8

19980720 100

DOE